Development 140, 3244-3253 (2013) doi:10.1242/dev.093278

Short-lived Her proteins drive robust synchronized oscillations in the zebrafish segmentation clock

Ahmet Ay[1,2,*], Stephan Knierer[3,‡], Adriana Sperlea[4,‡], Jack Holland[4,‡] and Ertuğrul M. Özbudak[3,*]

SUMMARY

Oscillations are prevalent in natural systems. A gene expression oscillator, called the segmentation clock, controls segmentation of precursors of the vertebral column. Genes belonging to the *Hes/her* family encode the only conserved oscillating genes in all analyzed vertebrate species. Hes/Her proteins form dimers and negatively autoregulate their own transcription. Here, we developed a stochastic two-dimensional multicellular computational model to elucidate how the dynamics, i.e. period, amplitude and synchronization, of the segmentation clock are regulated. We performed parameter searches to demonstrate that autoregulatory negative-feedback loops of the redundant repressor Her dimers can generate synchronized gene expression oscillations in wild-type embryos and reproduce the dynamics of the segmentation oscillator in different mutant conditions. Our model also predicts that synchronized oscillations can be robustly generated as long as the half-lives of the repressor dimers are shorter than 6 minutes. We validated this prediction by measuring, for the first time, the half-life of Her7 protein as 3.5 minutes. These results demonstrate the importance of building biologically realistic stochastic models to test biological models more stringently and make predictions for future experimental studies.

KEY WORDS: Segmentation clock, Oscillation, Protein half-life, Systems biology, Computational modeling, Zebrafish

INTRODUCTION

Oscillatory systems pervade biology on every scale. Predator-prey population dynamics, daily rhythms of organisms and developmental pattern formation all show oscillatory behavior over periods of time. The anterior-posterior body axis of vertebrates is patterned as a series of spatially repetitive somite segments. As cells emerge from the presomitic mesoderm (PSM), located at the growing posterior end of the embryo, they are grouped together and organized into segments known as somites that will later differentiate into the vertebral column and trunk, and limb muscle tissues (Pourquié, 2011).

The periodicity of somite segmentation is controlled by a gene-expression oscillator, called the segmentation clock, which ticks in the cells of the unsegmented mesoderm. The oscillation period of the segmentation clock dictates the period of somite segmentation. Breakdown of oscillations disrupts somite segmentation and results in vertebral defects (Pourquié, 2011). Somite segmentation, i.e. somitogenesis, occurs in all vertebrates and has been experimentally studied in many species (Gomez et al., 2008; Eckalbar et al., 2012).

Hairy/enhancer-of-split-related genes (called *Hes/her* genes) are the only conserved oscillating genes in all studied species (Krol et al., 2011; Eckalbar et al., 2012). In zebrafish, the genes thought to be involved in somitogenesis that show oscillatory expression in the posterior PSM include *her1*, *her7* and *deltaC* (Ozbudak and Pourquié, 2008) (Fig. 1). *her1* and *her7* genes encode members of the basic helix-loop-helix (bHLH) family of transcription factors; they function as transcriptional repressors only following dimerization. *deltaC* encodes a ligand for the Notch receptor. Hes6 protein (also called Her13.2) belongs to the same bHLH family of repressors as Her1 and Her7, but its expression does not oscillate, unlike Her1 and Her7 (Kawamura et al., 2005). Her1, Her7 and Hes6 proteins form homo- and heterodimers at different levels (Schröter et al., 2012; Trofka et al., 2012; Hanisch et al., 2013), and these dimers repress transcriptions of *her1*, *her7* and *deltaC* (Giudicelli et al., 2007) forming a negative-feedback loop that has the potential to create oscillatory gene expression. It is the oscillatory expression patterns of these transcriptional repressors within the PSM that are proposed to be the mechanism underlying the segmentation clock (Lewis, 2003). Each oscillatory cycle defines a new somite and individual cellular positioning within that somite depends on the corresponding phase of the cycle during which each cell was generated. Delta-Notch signaling enhances the transcription of *her1* and *her7* and ensures their oscillations are synchronized across neighboring cells (Jiang et al., 2000; Horikawa et al., 2006; Mara et al., 2007; Riedel-Kruse et al., 2007; Ozbudak and Lewis, 2008; Delaune et al., 2012) (Fig. 1).

Mathematical models have been employed frequently to obtain a mechanistic understanding of this fascinating developmental clock and shed light on its counterparts in different organisms. Ozbudak and Lewis (Ozbudak and Lewis, 2008) modeled the system using only *her1*, *her7* and *deltaC* genes in a two-cell system at the posterior PSM. Cinquin (Cinquin, 2007) modeled the same system using *her1*, *her7*, *hes6* and *deltaC* genes in a one-dimensional chain of cells. Both of these models were built on experimental data that have been extensively updated recently. The system has been recently modeled by Schröter et al. (Schröter et al., 2012) and Hanisch et al. (Hanisch et al., 2013). Although the model published by Schröter et al. matched some current experimental findings, it is a simplified deterministic model, concentrating only on a single cell and approximating dimerization of proteins rather than explicitly including dimer species. Owing to its simplicity, this model could not address the phenotypes observed with loss of Notch signaling (such as loss of synchrony among oscillations of neighboring cells, reduction in oscillation amplitude and increase in oscillation period). Furthermore, this model could not predict how synchronization is

[1]Department of Mathematics, Colgate University, Hamilton, NY 13346, USA. [2]Department of Biology, Colgate University, Hamilton, NY 13346, USA. [3]Department of Genetics, Albert Einstein College of Medicine, Bronx, NY 10461, USA. [4]Department of Computer Science, Colgate University, Hamilton, NY 13346, USA.

‡These authors contributed equally to this work
*Authors for correspondence (aay@colgate.edu; ertugrul.ozbudak@einstein.yu.edu)

Accepted 17 May 2013

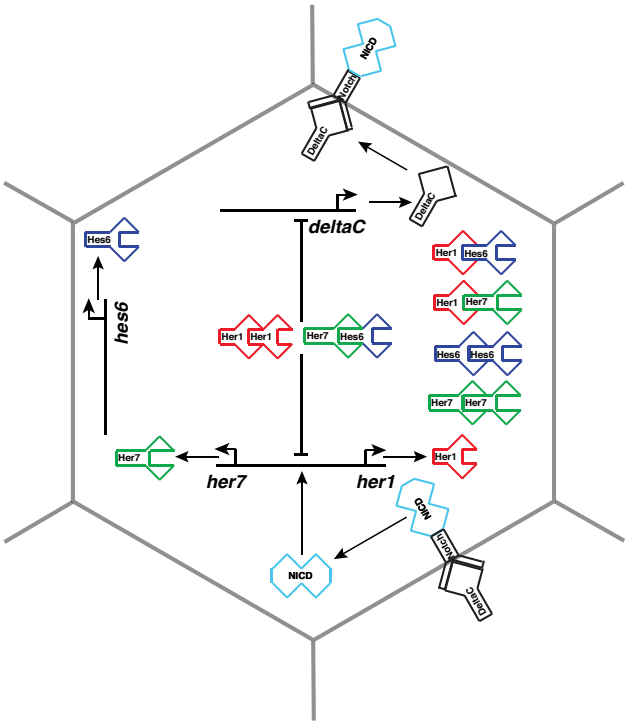

Fig. 1. Model of the interactions between Her proteins in the zebrafish segmentation network. Her1, Her7 and Hes6 can form homo- and heterodimers. However only Her1-Her1 homodimer and Her7-Hes6 heterodimer bind to the enhancer region of the *her1*, *her7* and *deltaC* genes and regulate their transcription. Intercellular communication occurs through Notch signal transduction pathway, which enhances *her1* and *her7* transcription.

affected in the mutants of *her* family genes. Hanisch et al. modeled the system at the multicellular level, but this model did not address the mutant phenotypes of all *her* family genes (such as the $hes6^{-/-}$ and $her7^{-/-};hes6^{-/-}$ mutants) and the change in the period of segmentation when Notch signaling was impaired.

In the present study, we extended these earlier models by building a multicellular stochastic computational model for the oscillations taking place at the posterior PSM. Our simulations demonstrated that a modified version of a mathematical model based on a simple autoregulatory feedback loop (Lewis, 2003) can accommodate the experimental observations (Jiang et al., 2000; Horikawa et al., 2006; Mara et al., 2007; Riedel-Kruse et al., 2007; Ozbudak and Lewis, 2008; Herrgen et al., 2010; Delaune et al., 2012; Schröter et al., 2012; Trofka et al., 2012; Hanisch et al., 2013). The autoinhibitory negative-feedback loops composed of two redundantly acting repressor dimers are sufficient to generate synchronized oscillations in wild-type embryos and we found parameter ranges that reproduce how the dynamics (i.e. period, amplitude and synchronization) of the segmentation oscillator are modified in different genetic backgrounds.

Previously, it has been proposed that the oscillating Her/Hes proteins should be short-lived for sustained oscillations to occur (Lewis, 2003). The half-life of mouse Hes7 protein was measured as 22 minutes in cell culture. Mutations that increase half-life of Hes7 disrupted oscillations and resulted in vertebral defects in mice (Hirata et al., 2004). Using our model, we randomly varied the biochemical parameters in biologically reasonable ranges and identified parameter sets that result in sustained synchronized oscillations in wild-type embryos and respective period, amplitude or synchronization changes in various mutant conditions. In all the identified parameter sets, half-life of Her proteins were shorter than 6.2 minutes, a rate that is roughly one quarter of the measured degradation rate in mice. We tested the prediction of our model by measuring the half-life of Her7 protein in a transgenic animal that can express an HA-tagged version of Her7 protein in an inducible manner. We found the half-life of HA-Her7 to be 3.5 minutes, matching the prediction of our model.

MATERIALS AND METHODS

Deterministic model

We have developed a time-delayed differential equation (DDE) model consisting of 14 equations with 44 parameters. Each equation describes the rate of change of an mRNA, monomer protein or dimer protein.

The variables: mh_i where $i \in \{1, 7, 6\}$ and md represent the number of mRNA molecules of *her1*, *her7*, *hes6* and *deltaC*, respectively; ph_i where $i \in \{1, 7, 6\}$ and pd represent the number of protein molecules of Her1, Her7, Hes6 and DeltaC, respectively; and $ph_{i,j}$ where $i \le j$ and $i,j \in \{1, 7, 6\}$ represent the number of molecules of Her1-Her1, Her1-Her7, Her1-Hes6, Her7-Her7, Her7-Hes6 and Hes6-Hes6 dimers. Each term in the model represents a rate of change for a biological reaction. Protein synthesis and degradation rates are described by psh_i, pdh_i where $i \in \{1, 7, 6\}$, psd and pdd for Her1, Her7, Hes6 and DeltaC, respectively. mRNA synthesis and degradation rates are described by msh_i, mdh_i where $i \in \{1, 7, 6\}$, msd and mdd for *her1*, *her7*, *hes6* and *deltaC*, respectively. Dimer association, dissociation and degradation rates for Her1-Her1, Her1-Her7, Her1-Hes6, Her7-Her7, Her7-Hes6 and Hes6-Hes6 are represented by $dah_{i,j}$, $ddh_{i,j}$ and $pdh_{i,j}$ where $i \le j$ and $i,j \in \{1, 7, 6\}$, respectively. DNA-binding dissociation constraints are $critph_{1,1}$, $critph_{6,7}$ and critpd, for Her1-Her1, Her7-Hes6 and Notch (NICD), respectively. Transcriptional and translational delays are represented by nmh_i where $i \in \{1, 7\}$, nph_i where $i \in \{1, 7, 6\}$, nmd and npd for *her1*, *her7*, *hes6* and *deltaC*, respectively. In the model equations below, we represent the k^{th} cell as c_k and time as t.

Deterministic equations

Monomer protein levels

Monomer equations describe the rate of change of monomers using translation, degradation, dimer association and dimer dissociation reactions. In the Her/Hes monomer equations, the synthesis and degradation reactions are factored in the first two terms in equations, and dimer association and dissociation reactions are factored in the third term. Her1, Her7 and Hes6 proteins form homo- and heterodimers (Schröter et al., 2012; Trofka et al., 2012; Hanisch et al., 2013). The time needed to translate mRNA is accounted for by the translational delay terms (Jensen et al., 2003; Lewis, 2003; Monk, 2003). Following Lewis (Lewis, 2003), the time delay in the activation of the Notch receptor is implicitly incorporated into the DeltaC protein production delay. The DeltaC monomer equation only contains the synthesis and degradation reactions.

$$\frac{\partial ph_i(c_k,t)}{\partial t} = psh_i \cdot mh_i(c_k, t - nph_i) - pdh_i \cdot ph_i(c_k,t) + \sum_{\substack{i\le j \text{ and} \\ i,\, j\in\{1,7,6\}}} C_{i,j} \cdot \left[ddh_{i,j} \cdot ph_{i,j}(c_k,t) - dah_{i,j} \cdot ph_i(c_k,t) \cdot ph_j(c_k,t) \right], \quad (1)$$

and

$$\frac{\partial pd(c_k,t)}{\partial t} = psd \cdot md(c_k, t - npd) - pdd \cdot pd(c_k,t), \quad (2)$$

where $C_{i,j} = 1$ if $i \neq j$, and $C_{i,j} = 2$ if $i = j$.

Dimer protein levels

Equations for the dimer proteins describe the rate of change of dimer levels using dimer association and dissociation (first and second terms), and degradation reaction (third term).

$$\frac{\partial ph_{i,j}(c_k,t)}{\partial t} = dah_{i,j} \cdot ph_i(c_k,t) \cdot ph_j(c_k,t) - ddh_{i,j} \cdot ph_{i,j}(c_k,t) - pdh_{i,j} \cdot ph_{i,j}(c_k,t), \quad (3)$$

where $i \le j$ and $i,j \in \{1, 7, 6\}$.

mRNA levels

mRNA equations describe the rate of change of mRNA levels using transcription and degradation reactions. Only Her1-Her1 and Her7-Hes6 dimers can bind to sites on the promoter regions of *her1*, *her7* and *deltaC* genes (Schröter et al., 2012; Trofka et al., 2012) to repress their transcription (Fig. 1), which is described in the first terms of the mRNA equations for *her1*, *her7* and *deltaC*. Transcriptional activation due to Delta-Notch signaling is reflected in the numerator of the transcription terms for *her1* and *her7*. The amount of DeltaC protein indirectly influencing mRNA synthesis in neighboring cells via binding to the Notch receptor is calculated as the average of DeltaC levels in all the neighbors with which a cell communicates. Cells were modeled to be hexagonal, resulting in six neighbors for each cell (Fig. 1). In contrast to *her1*, *her7* and *deltaC*, *hes6* mRNA is assumed to be constantly expressed.

$$\frac{\partial \mathrm{mh_i}(\mathrm{c_k},t)}{\partial t}=\mathrm{msh_i}\frac{1+\frac{1}{6}\sum_{\mathrm{c_n}\in N}\frac{\mathrm{pd}(\mathrm{c_n},t-\mathrm{nmh_i})}{\mathrm{critpd}}}{1+\frac{1}{6}\sum_{\mathrm{c_n}\in N}\frac{\mathrm{pd}(\mathrm{c_n},t-\mathrm{nmh_i})}{\mathrm{critpd}}+\left[\frac{\mathrm{ph_{1,1}}(\mathrm{c_k},t-\mathrm{nmh_i})}{\mathrm{critph_{1,1}}}\right]^2+\left[\frac{\mathrm{ph_{6,7}}(\mathrm{c_k},t-\mathrm{nmh_i})}{\mathrm{critph_{6,7}}}\right]^2}$$
$$-\mathrm{mdh_i}\cdot\mathrm{mh_i}(\mathrm{c_k},t), \quad (4)$$

where N represents all the neighbors of the k^{th} cell (c_k) and $i \in \{1, 7\}$,

$$\frac{\partial \mathrm{mh_6}(\mathrm{c_k},t)}{\partial t}=\mathrm{msh_6}-\mathrm{mdh_6}\cdot\mathrm{mh_6}(\mathrm{c_k},t), \quad (5)$$

and

$$\frac{\partial \mathrm{md}(\mathrm{c_k},t)}{\partial t}=\mathrm{msd}\cdot\frac{1}{1+\left[\frac{\mathrm{ph_{1,1}}(\mathrm{c_k},t-\mathrm{nmd})}{\mathrm{critph_{1,1}}}\right]^2+\left[\frac{\mathrm{ph_{6,7}}(\mathrm{c_k},t-\mathrm{nmd})}{\mathrm{critph_{6,7}}}\right]^2}$$
$$-\mathrm{mdd}\cdot\mathrm{md}(\mathrm{c_k},t). \quad (6)$$

Detailed descriptions of these equations and their derivations are provided in supplementary material Appendix S1.

Stochastic equations

The stochastic equations have been written as a direct translation of the deterministic model described above (supplementary material Appendix S1). All reactions were executed following an exponential law for which the reaction rate was the same as its deterministic counterpart. Similar to the deterministic model, protein-DNA binding and unbinding events (very fast compared with other events) have not been explicitly modeled. This is because reactions occurring on slower time scales (such as synthesis and degradation of mRNAs and proteins) smoothen the noise stemming from the reactions with fast dynamics (such as protein-DNA interactions) (Paulsson, 2004).

Deterministic and stochastic simulations

The deterministic simulation in our study is used to find biologically realistic parameter sets. The deterministic model is solved numerically using Euler's method. Euler's method increments the time in the chosen step size (e.g. 0.01 minutes), and updates mRNA and protein levels at each iteration using the rate of changes provided by the model. The stochastic simulations in our study are performed using the next reaction method (NRM), which discretely computes concentration levels based on probabilistic calculations (Anderson, 2007). Probabilistically determined propensities and reaction times are used to decide which reaction fires at each iteration. Reactions with higher propensities are more likely to fire. A delayed reaction queue is incorporated into the standard NRM algorithm to accommodate time delays (Anderson, 2007). Each iteration in NRM is computed as follows:

1. Update the propensity values related to the most recently fired reaction for each cell.
2. Calculate the time gap (the size of the next time step) using propensities.
3. Increment the time step and the relevant molecular counts.
4. If a delayed reaction is initiated, add it to the appropriate list. Otherwise fire immediate reactions and delayed reactions that are finished.
5. Repeat until simulation time expires.

Parameter search

Upper limits for the mRNA decay rates and transcriptional time-delays were measured previously (Giudicelli et al., 2007). However, most of the reaction rates in the segmentation clock network have not been experimentally measured precisely owing to technical difficulties. We have employed a parameter search to identify parameter values that were capable of reproducing experimental observations.

Initial parameter sets were composed of randomly generated parameter values (within biologically relevant ranges) (supplementary material Table S1) and deterministic simulations were then run with the resulting parameters. Initial parameter ranges using deterministic simulations have been constrained by comparison with experimental period observations for wild type, and *her1*$^{-/-}$, *her7*$^{-/-}$, *hes6*$^{-/-}$, *her7*$^{-/-}$;*hes6*$^{-/-}$ and *notch1a*$^{-/-}$ mutant zebrafish embryos (supplementary material Table S1). Approximately 5,000,000 parameter sets were run, with 200,000 passing the initial criteria on period restrictions. These 200,000 parameter sets were run with the NRM stochastic algorithm. The same restrictive period values were used to find the parameter sets that also worked for the two-cell stochastic simulations, resulting in a smaller number of parameter sets. The parameter values were further pruned by comparison to the experimental data on synchronization and amplitude of oscillations using two-cell stochastic simulations. Finally, the parameter sets that passed all of the previous steps (~200) were used to run our stochastic simulation code for a sixteen-cell tissue (4×4). The simulations are compared with the current experimental data on period, synchronization and amplitude of oscillations in different genetic backgrounds. Only 41 parameter sets have passed these final criteria.

Oscillation features

Deterministic simulations

The last peak and trough of the *her1* mRNA oscillations were used to calculate the period and amplitude of the oscillations. Period was calculated as the time difference between the last two peaks, and amplitude was calculated as the expression level change between the last peak and trough.

Stochastic simulations

Calculation of oscillation features in the stochastic simulations was performed slightly differently owing to the noise in the resulting data. The first step in the calculation was smoothing the data using a 40 time step moving average method. Keeping the smoothing interval small did not affect the accuracy of the results. Because the peaks and troughs vary across the data, all the local maxima and minima were used as peak and trough values. A value more than five values to its left and five to its right was considered a local maximum, and a value less than five values to its left and five to its right was considered a local minimum. For every peak-trough pair, the value of the period and amplitude was calculated. To obtain an overall value of the period and amplitude for a run, these values were then averaged, and then averaged again over the number of runs when doing multiple runs.

In the stochastic simulations, the measure of synchronization was calculated using Pearson's correlation coefficient. Within one run, the score was the average of the correlation coefficients between each cell and the first cell. For multiple runs, the average of the individual scores for each run was used.

We have used Student's *t*-test to calculate *P* values and to determine the statistical significance of our results throughout the paper.

Coding

The codes for the study have been implemented in C++ and Python (available upon request). C++ was used because of its speed and Python because of its easy-to-use plotting libraries. The current version of our code can finish 1200 minutes of deterministic and stochastic simulations for a 16-cell tissue in less than a minute and four hours, respectively (on a node containing two quad-core Xeons at 2.3 GHz, 8 GB of memory). Parallel versions of the code have been written in order to run time-intensive stochastic simulations in parallel in a scientific cluster.

Measurement of protein stability

Heterozygous *Tg(hsp70l:HA-her7)* (Giudicelli et al., 2007) zebrafish embryos of ~12-14 somite stages were dechorionated manually and heat shocked in a water bath for 1 hour at 37°C. Animals were then placed back in fish water at 24°C to recover for 5 minutes and then transferred to embryo media containing 100 μg ml^{-1} cycloheximide for 15 minutes of incubation. For each measuring time point, 15 embryos were collected every 2.5 minutes and deyolked in 1 ml ice cold 1×Ringer's solution without calcium using a glass Pasteur pipette. Embryos were then harvested by centrifugation at 350 ***g*** for 30 seconds at room temperature and supernatant was carefully taken off. The resulting cellular fractions were suspended in 48 μl protein lysis buffer [50 mM Tris-HCl, pH 7.4, 100 mM NaCl, 5 mM $MgCl_2$, 0.5 mM EDTA, 0.1% Triton X-100, supplemented with 10×EDTA-free protease inhibitor cocktail (Roche), 10 mg ml^{-1} pepstatin, 10 mM sodium pyrophosphate pH 7.5, 10 mM β-glycerophosphate pH 7.5, 10 mM NaF] containing 250 U ml^{-1} nuclease (Thermo Fisher) and subsequently lysed by adding 12 μl 5×SDS Laemmli protein sample buffer. Samples were immediately frozen in liquid nitrogen for storage.

For western blot analysis, the total protein extracts were heated at 85°C for 5 minutes and loaded at volumes of 37.5 μl (corresponding approximately to nine embryos) on 4-15% gradient gels and blotted overnight to PVDF membranes. Immunodetection of HA-Her7 proteins was carried out using mouse anti-HA (Roche 12CA5) and HRP-conjugated anti-mouse secondary antibodies. Relative amounts of detected HA-Her7 proteins were quantified after imaging using ImageJ (NIH) software.

RESULTS

Stochastic modeling assesses the validity of biological cartoon models more faithfully than its deterministic counterpart

Biological systems are often analyzed using deterministic simulations in which the input variables entirely determine the output. However, biological reactions are inherently noisy (stochastic) (Ozbudak et al., 2002). Stochastic simulations reflect this randomness by allowing random fluctuations to influence the output of biological processes. Thus, biological systems should be analyzed with stochastic models to capture a faithful representation of the systems. Furthermore, gene expression noise poses a great challenge to maintain the synchrony among oscillating neighboring cells in the segmentation clock (Riedel-Kruse et al., 2007; Ozbudak and Lewis, 2008; Delaune et al., 2012). Therefore, to obtain a more accurate description of this system and to determine how the synchronization of oscillations is affected when different genes in the segmentation clock network were mutated, we have utilized stochastic simulations.

The multicellular model reproduces the changes in segmentation period in six different genetic backgrounds

Previous studies demonstrate that double knockdown of two oscillating genes, *her1* and *her7*, prevents somite segmentation (Henry et al., 2002; Oates and Ho, 2002; Gajewski et al., 2003). The period of segmentation does not change in the single $her1^{-/-}$ or $her7^{-/-}$ mutants (Schröter et al., 2012; Hanisch et al., 2013). $hes6^{-/-}$ and $her7^{-/-};hes6^{-/-}$ mutants do not have any segmentation defect (Sieger et al., 2006; Schröter et al., 2012; Trofka et al., 2012), but the period of the oscillations is increased by ~6% (Schröter and Oates, 2010; Schröter et al., 2012). Double knockdown of *her1* and *hes6* also prevents somite segmentation. Mutations of genes involved in Notch signaling increases the period of segmentation by ~7-23% over wild type (Herrgen et al., 2010). Our stochastic model demonstrates that the current zebrafish segmentation clock network is able to explain all quantitative experimental observations in wild type and $her1^{-/-}$, $her7^{-/-}$, $hes6^{-/-}$, $her7^{-/-};hes6^{-/-}$ and $notch1a^{-/-}$ mutant embryos. We present synchronization (Fig. 2), period (Fig. 3) and amplitude (Fig. 4) values obtained for the *her1* mRNA levels by our model. These values are similar for *her7* mRNA levels.

Our model predicts a period of ~31-32 minutes for *her1* mRNA oscillations in wild-type embryos, a similar period in $her1^{-/-}$ and $her7^{-/-}$ (P=1 and 0.1, respectively), ~5.7% increase in $hes6^{-/-}$ ($P=5\times10^{-8}$), 5.8% increase in $her7^{-/-};hes6^{-/-}$ ($P=5.8\times10^{-9}$) and 8.5% increase in $notch1a^{-/-}$ ($P=6.5\times10^{-8}$) mutant embryos (Figs 3, 5). *her1* mRNA oscillations are lost in $her1^{-/-};her7^{-/-}$ and $her1^{-/-};hes6^{-/-}$ double mutants. This is an obvious consequence of our model in which only Her1-Her1 and Her7-Hes6 dimers repress transcription of *her1*, *her7* and *deltaC*. These are all in agreement with current experimental findings.

Stochastic simulations predict how synchronization of oscillations will be affected when various genes are mutated in the segmentation clock network

The segmentation clock is synchronized across neighboring cells via the Delta-Notch signal transduction pathway (Jiang et al., 2000; Horikawa et al., 2006; Mara et al., 2007; Riedel-Kruse et al., 2007; Ozbudak and Lewis, 2008; Delaune et al., 2012); synchronized gene expression is lost among neighboring cells when Notch signaling is impaired, which has been reproduced by our model ($P=4\times10^{-31}$) (Figs 2, 5; supplementary material Movies 1-6).

$her7^{-/-}$ mutant embryos exhibit segmentation defects that are confined to the posterior axis (Choorapoikayil et al., 2012; Schröter et al., 2012; Hanisch et al., 2013). Our model shows that synchronized gene expression among cells has been impaired in these embryos in comparison with wild type ($P=2.8\times10^{-19}$) (Figs 2, 5). Somites segment properly in $her1^{-/-}$, $hes6^{-/-}$ and $her7^{-/-};hes6^{-/-}$ mutants (Sieger et al., 2006; Schröter et al., 2012; Trofka et al., 2012; Hanisch et al., 2013). Our simulations show that synchronized gene expression among cells in $her1^{-/-}$, $hes6^{-/-}$ and $her7^{-/-};hes6^{-/-}$ mutants is preserved, similar to wild-type embryos (P=0.5, 0.9 and 0.1, respectively) (Figs 2, 5).

Changes in the amplitude of oscillations in various genetic backgrounds is explained by the multicellular model

A critical amplitude of gene expression oscillations is important for proper segment formation. It has been shown that, when Notch signaling is blocked with the inhibitor DAPT, the amplitude of *her1* mRNA expression is decreased by ~20% (Ozbudak and Lewis, 2008). In close agreement, our model provides an average decrease of ~17% ($P=6.3\times10^{-5}$) (Figs 4, 5). The amplitude of *her1* mRNA expression is similar in $her1^{-/-}$ mutant embryos to that in the wild-type embryos, which is reproduced in our model (P=0.7). Our model provides an explanation for the observation $her7^{-/-}$ mutant embryos show defects in somite formation, suggesting that this might be due to reduction in amplitude and partial loss of synchronization among neighboring cells. Our simulations show that the amplitude of *her1* mRNA expression decreases by ~21% in $her7^{-/-}$ mutant embryos in comparison with wild-type embryos ($P=4.3\times10^{-7}$) (Figs 4, 5). Forty-one parameter sets satisfied all the experimentally observed changes in the period, amplitude or synchronization of oscillations in all mutant conditions. In 29 of these parameter sets, the amplitude of oscillations in single cells is reduced by >15% in $her7^{-/-}$ mutants, in 31 of them synchronization is lost by >15% in $her7^{-/-}$ mutants, and in 26 of

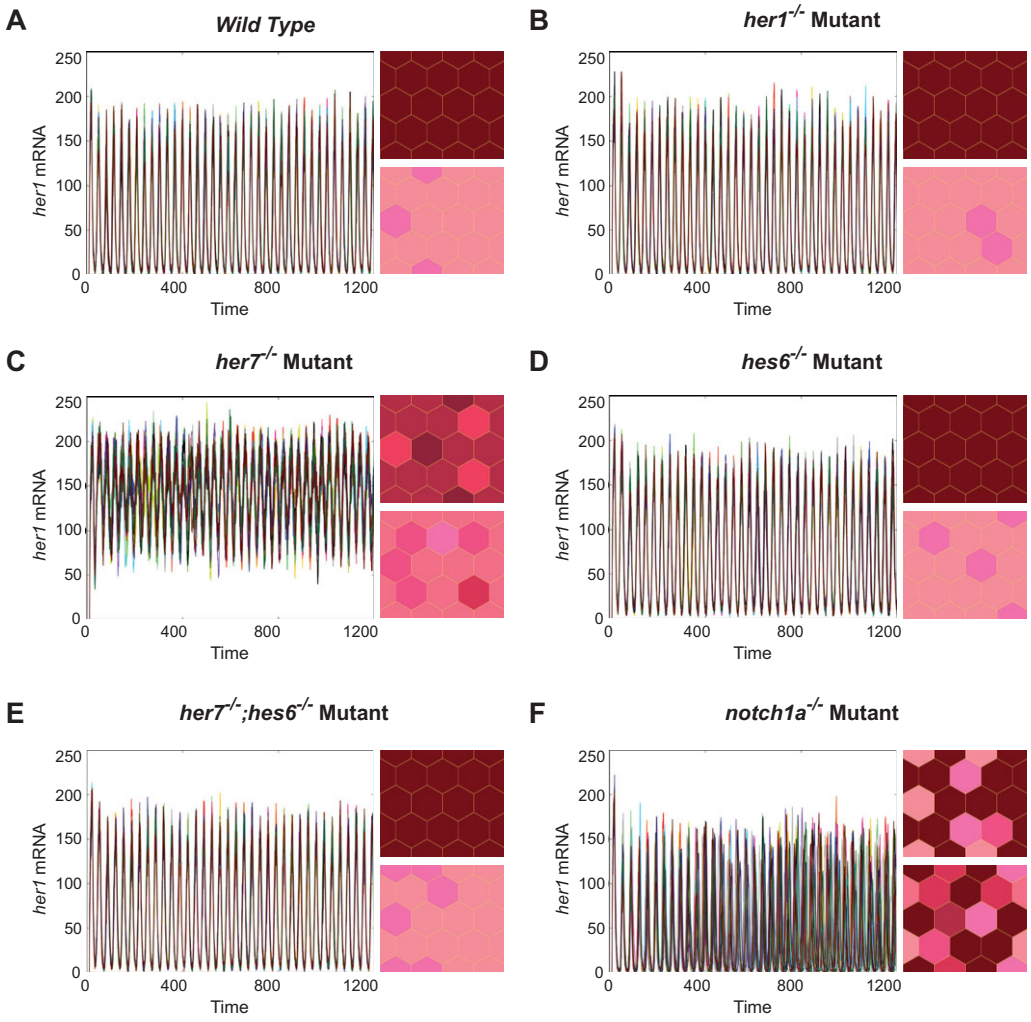

Fig. 2. Synchronization of oscillations for a selected parameter set. (**A-F**) *notch1a*$^{-/-}$ and *her7*$^{-/-}$ mutants lose synchrony among cells. *her1* mRNA levels for 16 cells (4×4 tissue) have been plotted for the first 1200 minutes of the wild type and *her1*$^{-/-}$, *her7*$^{-/-}$, *hes6*$^{-/-}$, *her7*$^{-/-}$;*hes6*$^{-/-}$ and *notch1a*$^{-/-}$ mutants for a selected parameter set. *her1* mRNA expression levels for the 4×4 tissue are shown as snapshots for two time points of the wild type and *her1*$^{-/-}$, *her7*$^{-/-}$, *hes6*$^{-/-}$, *her7*$^{-/-}$;*hes6*$^{-/-}$ and *notch1a*$^{-/-}$ mutants. Each hexagon represents a cell, with its color indicating its level of *her1* mRNA. Darker colors indicate lower levels, whereas lighter colors represent higher levels. *notch1a*$^{-/-}$ mutants lose synchrony over time owing to loss of the intercellular communication via the Notch signaling pathway (F). Interestingly, *her7*$^{-/-}$ mutants show a similar behavior to *notch1a*$^{-/-}$ mutants, but not as severe (C). *her1* mRNA levels remain approximately the same in the wild type and *her1*$^{-/-}$, *hes6*$^{-/-}$, *her7*$^{-/-}$;*hes6*$^{-/-}$ mutant embryos at any given point with small variations due to the stochastic nature of the simulations (>0.9 correlation score).

them amplitude is reduced and synchronization is decreased by >15% in *her7*$^{-/-}$ mutants in comparison with wild-type embryos. Experimental studies suggest that the amplitude of *her1* mRNA expression is similar in *hes6*$^{-/-}$ and *her7*$^{-/-}$;*hes6*$^{-/-}$ mutant embryos to that in wild-type embryos (Schröter et al., 2012); our model reproduces this result with only an insignificant increase in amplitude: ~2% in *hes6*$^{-/-}$ and ~3% in *her7*$^{-/-}$;*hes6*$^{-/-}$ mutants (P=0.6 and 0.4, respectively) (Fig. 5).

The half-life of Her7 protein is very short, as predicted by the stochastic model

The existence of sustained oscillations depends on the half-lives of oscillating mRNA and proteins (Lewis, 2003). An upper limit of 6-8 minutes was previously calculated for the half-lives of *her1*, *her7* and *deltaC* mRNAs (Giudicelli et al., 2007). In our parameter searches, we obtained half-life parameters of between 2 and 6 minutes for these three mRNAs that satisfy the dynamic features of oscillations in all assessed genetic conditions. We calculated transcriptional time delays of 9-10 minutes for *her1*, *her7* and *deltaC* in our recent study (Hanisch et al., 2013). Here, we obtained parameters corresponding to a range of 6-12 minutes for the transcriptional time delays for these three genes to satisfy all the experimental conditions. Overall, our simulation results agree with the experimentally measured or estimated reaction rates. However, future studies that more precisely measure these biochemical rates as well as other so far unmeasured rates are needed.

To measure the third critical parameter, the half-life of Her proteins, we utilized a transgenic animal that can inducibly express HA-Her7 upon heat-shock treatment of embryos (Giudicelli et al., 2007). We administered an hour of heat shock, recovered embryos for 5 minutes at 24°C and incubated them with 100 μg/ml cycloheximide for 15 minutes before collecting embryos every

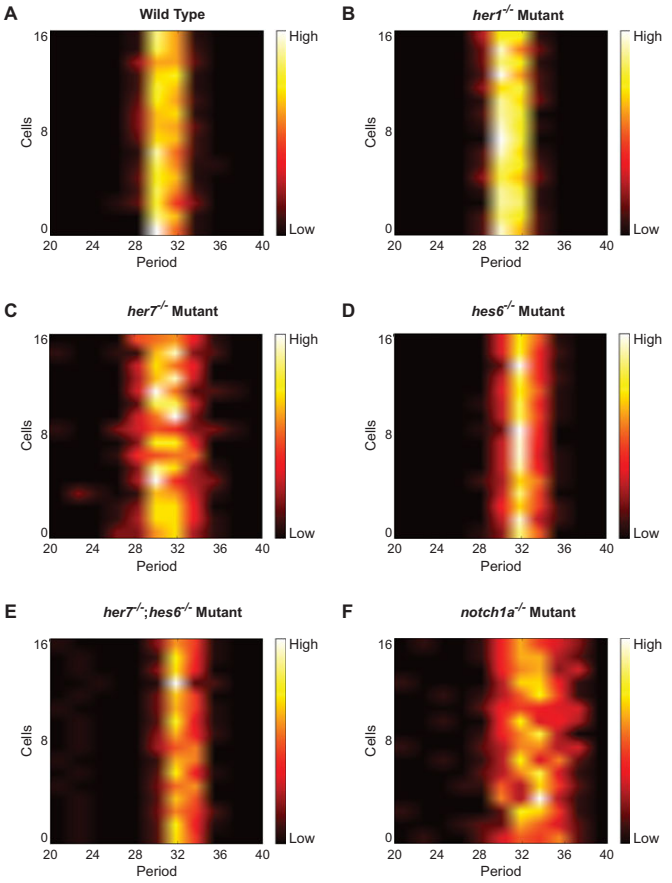

Fig. 3. Period of oscillations for a selected parameter set. (**A-F**) Heat maps for the stochastic simulations of the model, in which the *x*-axis represents the period (in minutes) and the *y*-axis represents the 16 cells. Lighter colors indicate higher densities of data points for the period of oscillations. For the selected parameter set, the average period for oscillations of the wild-type embryo in the first 1200 minutes is ~30 minutes (A), *her1*$^{-/-}$ and *her7*$^{-/-}$ mutants are same with wild type (B,C), *hes6*$^{-/-}$ and *her7*$^{-/-}$;*hes6*$^{-/-}$ mutants ~5.2% longer than wild type (D,E) and *notch1a*$^{-/-}$ mutant ~8.5% longer than wild type (F). Period predictions match the experimental findings and demonstrate that our model can describe the system accurately.

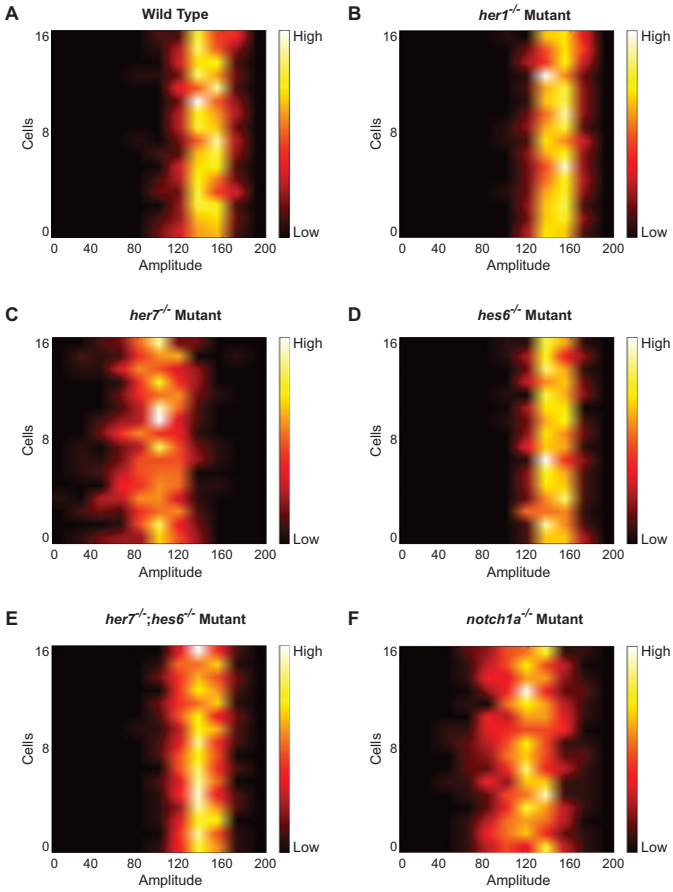

Fig. 4. Amplitude of oscillations for a selected parameter set. (**A-F**) Heat maps from the stochastic simulations of the model, in which the *x*-axis represents the amplitude and the *y*-axis represents the 16 cells. Lighter colors indicate higher densities of data points for the amplitude of oscillations. For the selected parameter set, the average amplitude for the oscillations of the wild-type embryo in the first 1200 minutes is 116 (A), *her1*$^{-/-}$ mutant embryo is 3% more than the wild type (B), *her7*$^{-/-}$ mutant is 18% less than the wild type (C), *hes6*$^{-/-}$ mutant is 14% more than the wild type (D), *her7*$^{-/-}$;*hes6*$^{-/-}$ mutant is 14% more than the wild type (E) and *notch1a*$^{-/-}$ mutant is 16% less than the wild type (F).

2.5 minutes. We then performed western blots using anti-HA antibodies to quantify Her7 abundance and used an exponential decay curve to determine the degradation rate of HA-Her7 protein. We measured the half-life of HA-Her7 as 3.5 minutes at 24°C (Fig. 6B). This rate is consistent with our simulation parameters, where we find the half-life of Her proteins between 1.8 and 6.2 minutes (average=3 minutes, standard deviation=1.1 minutes) (Fig. 6A).

DISCUSSION

Stochastic simulations validate all experimentally observed phenotypes

Somitogenesis is one of the best examples demonstrating the importance of developmental timing, and understanding this process in zebrafish lays the foundation for understanding it in more complex organisms. Experimental data have been obtained more quantitatively in recent years. We had previously measured the transcriptional time delays (Giudicelli et al., 2007; Hanisch et al., 2013) and obtained upper limits for the half-lives of *her1*, *her7* and *deltaC* mRNAs (Giudicelli et al., 2007). We further demonstrated that the amplitude of *her1* expression was reduced by ~20% when Notch signaling was blocked by treatment of the inhibitor DAPT (Ozbudak and Lewis, 2008). Recent measurements of changes in the segmentation period in *her1*$^{-/-}$, *her7*$^{-/-}$ (Schröter et al., 2012; Hanisch et al., 2013), *hes6*$^{-/-}$ and *her7*$^{-/-}$;*hes6*$^{-/-}$ (Schröter and Oates, 2010; Schröter et al., 2012) mutants provided quantitative data that could be utilized to build more realistic computational models.

In this study, we have modeled the zebrafish segmentation clock by focusing on the posterior PSM and using current knowledge of the segmentation clock network. Our stochastic multicellular model demonstrated that: (1) synchronized oscillations can be obtained in wild-type conditions; (2) the synchrony will be lost, the amplitude of oscillation will be reduced and the period of oscillation will be lengthened in *notch1a*$^{-/-}$ mutants; (3) the period of oscillation, the amplitude of oscillation and the synchronization of oscillations are not affected in *her1*$^{-/-}$ mutants; (4) oscillations are more sensitive to loss of *her7* as the amplitude and the synchronization of

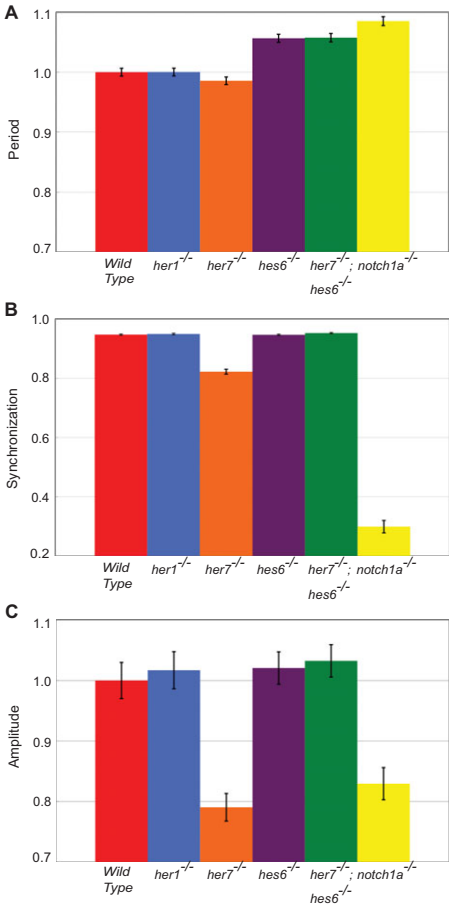

Fig. 5. The period, amplitude and synchronization scores for all parameter sets. (**A-C**) Bar graphs representing the average and standard error for the oscillation measures indicated. (A) Period measures for *her1*$^{-/-}$ and *her7*$^{-/-}$ mutants are same as wild type, *hes6*$^{-/-}$ and *her7*$^{-/-}$;*hes6*$^{-/-}$ mutants ~5.7% longer than wild type (P=5.03×10^{-8} and 5.77×10^{-8}, respectively), and *notch1a*$^{-/-}$ mutant ~8.5% longer than wild type (P=6.51×10^{-13}). (B) Synchronization is lost in *notch1a*$^{-/-}$ (mean=0.29 correlation score, P=3.53×10^{-31}) and reduced in *her7*$^{-/-}$ (mean=0.82 correlation score, P=2.81×10^{-19}) mutants in comparison with wild type (>0.9 correlation score). Synchronization levels are similar to the wild-type case for *her1*$^{-/-}$, *hes6*$^{-/-}$ and *her7*$^{-/-}$;*hes6*$^{-/-}$ mutants (P=0.54, 0.85 and 0.08, respectively). (C) Amplitude measures for *her1*$^{-/-}$, *hes6*$^{-/-}$ and *her7*$^{-/-}$;*hes6*$^{-/-}$ mutants are similar to wild type (P=0.69, 0.61 and 0.43, respectively), *her7*$^{-/-}$ mutants ~21% smaller than wild type (P=4.31×10^{-7}), and *notch1a*–/– mutant ~17% smaller than wild type (P=6.26×10^{-5}). Period, synchronization and amplitude predictions match the experimental findings, and demonstrate that our model can describe the system accurately.

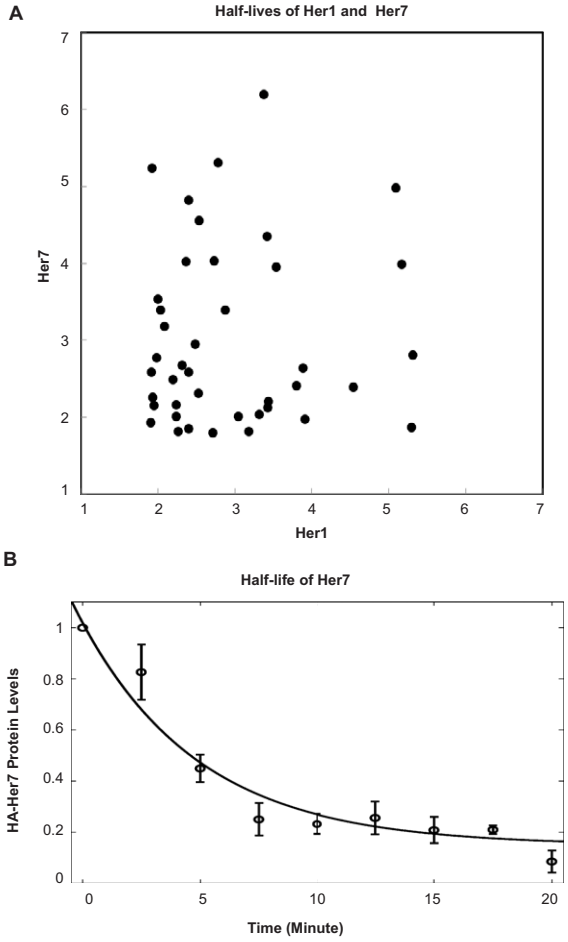

Fig. 6. Half-life prediction and experimental validation for Her proteins. (**A**) The half-life parameters of Her1 and Her7 proteins determined from the 41 parameter sets that have satisfied all the dynamic features of segmentation clock in stochastic simulations. (**B**) Experimental measurements match the model's predictions. The protein levels at later time points are normalized to that of the first time point for each experiment. The average normalized protein levels are plotted with the standard deviation. The exponential decay curve is plotted with a black line. The equation that gives the best fit (R^2 = 0.95) is $y = A{\cdot}e^{B{\cdot}t} + C$ where A = 0.8702, B = –0.1973 and C = 0.1482.

oscillations are reduced in *her7*$^{-/-}$ mutants; (5) the period of oscillations is not affected in *her7*$^{-/-}$ mutants; (6) the period of oscillations is lengthened in *hes6*$^{-/-}$ mutants; (7) the amplitude and the synchronization of oscillations are not affected in *hes6*$^{-/-}$ mutants; (8) the period change in the *her7*$^{-/-}$;*hes6*$^{-/-}$ mutant is similar to that of the *hes6*$^{-/-}$ mutant; (9) sensitization of the *her7*$^{-/-}$ mutant can be rescued by obtaining double *her7*$^{-/-}$;*hes6*$^{-/-}$ mutants as the amplitude and the synchronization of oscillations are not affected in *her7*$^{-/-}$;*hes6*$^{-/-}$ mutants; and (10) oscillations are abolished in *her1*$^{-/-}$;*her7*$^{-/-}$ or *her1*$^{-/-}$;*hes6*$^{-/-}$ double mutants.

Mutations in different *her/hes* genes result in distinctive phenotypes

Why do segmentation defects occur in the *her7*$^{-/-}$ mutant?

We and others have shown that some of the posterior somites segment but other somites fail to segment in *her7*$^{-/-}$ mutants (Choorapoikayil et al., 2012; Schröter et al., 2012; Hanisch et al., 2013). Our multicellular stochastic model captures this aspect accurately as it shows that the segmentation clock is sensitized against 'noise' in gene expression (Ozbudak et al., 2002) rather than damped out as previously claimed (Schröter et al., 2012). The synchronous oscillations are compromised; the synchrony levels fall below a threshold level during some of the oscillation cycles in a given embryo. But why does this happen? Figure 7A shows that the average DeltaC protein levels in *her7*$^{-/-}$ mutants are much higher than those in wild type and in other *her/hes* mutant backgrounds. This is due to *deltaC* being de-repressed during the 'off' phase of sensitized oscillations. This deficiency results in more-or-less continuous (small peak-to-trough) Delta-Notch

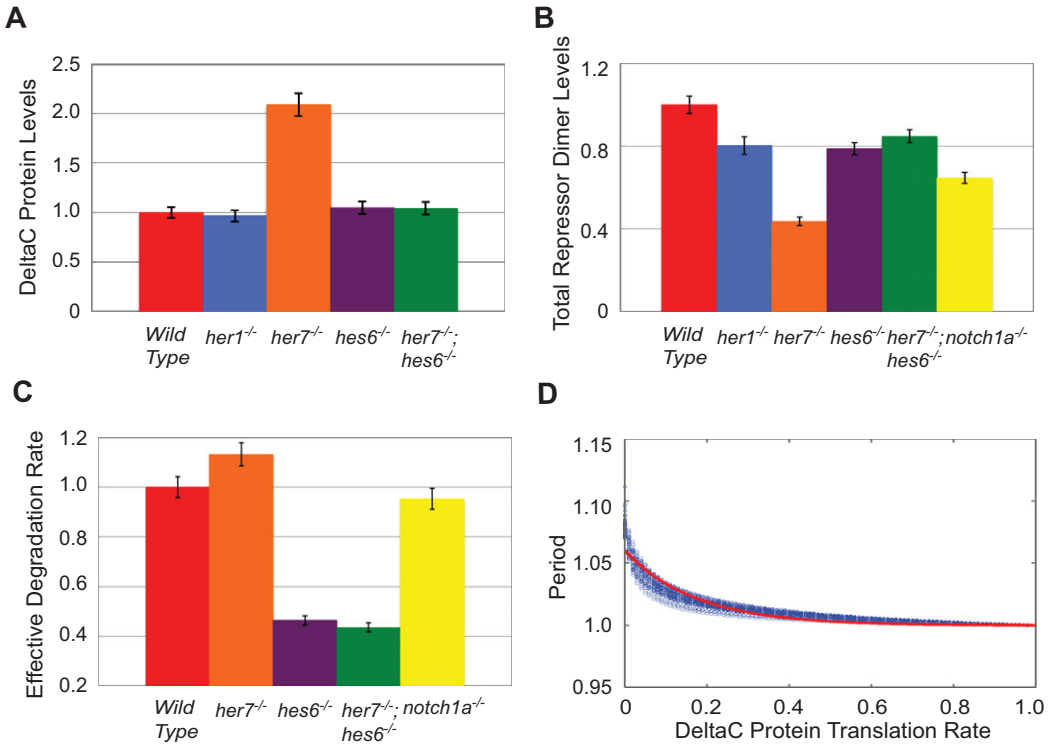

Fig. 7. System properties are selectively altered in different mutant backgrounds. (**A-C**) Normalized levels of DeltaC protein (A), total repressive dimers (B) and effective degradation rate of Her1 protein (C) in different genetic backgrounds are plotted. The heights of the bars represent the normalized and time-averaged levels, and the error bars represent the normalized standard errors. (**D**) Normalized period of the segmentation clock versus normalized DeltaC protein translation rate is plotted for each of the 41 parameter sets. The obtained period data can be fit ($R^2 = 0.91$) with a function of the form: Period = $A{\cdot}e^{B{\cdot}psd} + C$, where A = 1, B = –5.7791 and C, = 0.06.

signaling between the neighboring cells. In other words, cells fail to deliver information regarding their oscillation phase to their neighboring cells. Furthermore, in *her7*$^{-/-}$ mutants, more Hes6 proteins are free to dimerize with Her1 protein. This essentially creates an excess of Her1-Hes6 heterodimers that cannot bind to DNA targets (Schröter et al., 2012; Trofka et al., 2012). As a result, the total level of dimers that can repress transcription is reduced in comparison with wild type and other *her/hes* mutants (Fig. 7B). The amplitudes are in general lower because of the titration affect, as has been pointed out before (Schröter et al., 2012).

Why is the period of oscillations increased in *hes6*$^{-/-}$ and *her7*$^{-/-}$*;hes6*$^{-/-}$ mutants?

Binding of Hes6 increases the 'effective' degradation rates of Her1 and Her7 monomers. In other words, there are fewer Her1 or Her7 monomers available in the cell. Although the half-lives of Her proteins might not change in *hes6*$^{-/-}$ and *her7*$^{-/-}$*;hes6*$^{-/-}$ mutants, the outcome is equivalent to an increase in their half-lives, i.e. effectively there are more free Her1 (and Her7) proteins. Increasing the half-lives of oscillating proteins increases the period of oscillations (Lewis, 2003). The impact of Hes6 in reducing the levels of free Her monomers is strong because it is expressed continuously; hence, its average level is expected to be higher than those of Her1 and Her7. Our model agrees with previous assertions (Schröter et al., 2012) and shows that the effective levels of Her1 and Her7 are decreased in *Hes6* and *Her7;Hes6* mutants compared with other mutants (Fig. 7C; supplementary material Fig. S1).

Why is the period of oscillations increased in Notch-pathway mutants?

Lewis (Lewis, 2003) derived a closed-form equation describing the period of oscillations in a single-cell oscillator as being mainly determined by the time delays and half-lives. How the period of oscillations in the multicellular system changes with respect to the Notch-Delta synthesis rate remained to be determined. Here, we obtained a relationship between the period of oscillations and the rate of synthesis of Notch-Delta proteins by numerically fitting the results obtained in our model. Our results show that the period of oscillations versus the DeltaC translation rate fits to an exponentially decreasing function (Fig. 7D).

Briefly, our analysis goes beyond that of Hanisch et al. (Hanisch et al., 2013) in demonstrating how the period of segmentation changes when Notch signaling is impaired and how the period, synchronization and amplitude of oscillations are affected in *hes6*$^{-/-}$ and *her7*$^{-/-}$*;hes6*$^{-/-}$ mutants. We also go beyond the analysis of Schröter et al. (Schröter et al., 2012) in showing that synchronized robust oscillations can be generated in wild-type embryos by coupling oscillations of redundant repressor dimers in neighboring cells via Notch signaling. We also show how the period and amplitude of oscillations are affected in *notch1a*$^{-/-}$ mutant embryos, and how the synchronization of oscillations is affected in single and double mutants of *her* family genes.

The predictive capacity of a mathematical model is assessed by how well it can explain all the experimental data. In different biological systems, initial models developed to explain early experimental observations are often abandoned by the accumulation

of additional data. Likewise, the rapid increase in the amount of experimental data on somite segmentation places constraints on the success of mathematical models. By matching to all quantitative data obtained in various genetic backgrounds so far, our model strongly supports the pacemaker model for the zebrafish somite segmentation clock, which is based on autoregulatory negative-feedback loops of short-lived Her proteins.

Future experimental studies can be used to test and extend our computational model

In addition to matching recently obtained quantitative data, our model also makes further predictions for future experiments. For example, the amplitude changes in individual or double *her* mutants and the compromised synchrony in *her7*$^{-/-}$ mutants can be measured by using transgenic animals reporting oscillations in real time (Delaune et al., 2012) to test the predictions of our model.

There are important experimental questions that have not yet been quantitatively assessed and which could limit the predictive capacity of any computational model. First, the two DNA-binding Her dimer species (Her1-Her1 and Her7-Hes6) might not repress all the oscillating genes, particularly *her1*, *her7* and *deltaC*, with equal strength. DNA binding does not guarantee efficient repression, which might also depend on cooperativity among binding sites for repressors and competition among different DNA-binding transcription factors. Second, our model also excludes a number of other *her* family genes such as *her4*, *her12* and *her15*. Knockdown of these genes does not impact the segmentation process. However, they seem to contribute to stripy expression of oscillating genes in the anterior PSM (Shankaran et al., 2007). Hence, they might play auxiliary roles in segmentation. Generation of mutants for these genes and crossing them with *her1* or *her7* mutants would assess whether any of these genes contribute to the functional repressor pools in the system. Third, Delta proteins might dimerize and each homo- or heterodimer might have different activating or inhibitory roles on Notch signaling (Wright et al., 2011). This might explain the differences in the change of period among different Notch pathway mutants (Herrgen et al., 2010). Future quantitative data can be incorporated into our model to elucidate the differential changes of segmentation period in different mutants of genes influencing Notch signaling. Owing to these shortcomings, diverse parameter sets might be able to produce the same qualitative observations. However, if more quantitative data are produced, our model can be updated to narrow down the parameter ranges. As quantitative data are completely lacking for the processes ongoing in the anterior PSM, we chose to focus on modeling the segmentation clock in the posterior PSM. We plan to expand our model to accommodate processes taking place in the anterior PSM as quantitative data are produced.

Zebrafish Her7 protein is degraded at a sixfold faster rate than its ortholog in mouse

One of the key parameters that strongly influences the existence and period of oscillations is the half-life of oscillating Her proteins. This value had so far been missing in zebrafish, but was measured to be ~22 minutes for mouse Hes7 protein (Hirata et al., 2004). As the clock speed is much faster in zebrafish, even a half-life of 22 minutes will not allow oscillations to occur in zebrafish. Via exhaustive parameter searches, our model predicts an average half-life of ~3 minutes for Her proteins; occasionally we obtained half-lives of up to 6.2 minutes for Her7 protein that were able to satisfy the quantitative features of somite segmentation in all mutant backgrounds (Fig. 6A).

We utilized a transgenic animal in which HA-tagged Her7 (HA-Her7) can be inducibly expressed in zebrafish embryos (Giudicelli et al., 2007). Previously, HA-Her7 was demonstrated to decay at a near-uniform rate in all tissues in the embryo, suggesting that the half-life of Her7 could be roughly equal in all tissues. We induced expression of HA-Her7 in the embryos and treated embryos with cycloheximide (to arrest translation) and measured the half-life of HA-Her7 as 3.5 minutes (Fig. 6B). We noticed that the initial rapid decay in Her7 protein levels saturates at later time points. There are two potential causes of this observation. (1) If there is cooperative stability (Buchler et al., 2005), i.e. dimers decay slower than monomers, then dimer concentrations dominate at later stages (Momiji and Monk, 2008), which results in slower decay at later time points. (2) If the proteins triggering degradation of Her7 are also short-lived, cycloheximide treatment could prevent the replenishment of the degradation complex. These options will be investigated in future studies. The measured value has to be treated as an upper limit for the half-life of Her7 as: (1) we overexpressed the HA-Her7 protein above its normal levels, and (2) the short HA-tag might have mildly stabilized Her7 protein. Nevertheless, the measured half-life corroborates the prediction of our model.

The *her* autoinhibitory feedback loop could be the pacemaker of the zebrafish segmentation clock

Oscillators are one of the most common network modules that regulate the timing of biological processes. Mechanistic understanding of the segmentation clock will clearly shed light into the comprehension of oscillators in other biological systems. Our study provides a comprehensive tissue-level stochastic modeling of the system explaining the amplitude, period and synchronization dynamics of the zebrafish somite segmentation clock. Although direct proof for the *her* autoinhibitory feedback loop acting as the pacemaker of the zebrafish segmentation clock is still lacking, our multicellular stochastic model suggests that the transcriptional feedback-based model could be sufficient to describe the inner workings of the clock. As multiple oscillations are running in parallel in amniotes, it is not clear whether the segmentation clock is really based on a simple transcriptional feedback loop in either zebrafish or amniotes (reviewed by Ozbudak and Pourquié, 2008). Thus, direct experimental tests are necessary to assess the accuracy of transcriptional feedback-based models (such as Goldbeter and Pourquié, 2008) in all vertebrate model organisms.

Acknowledgements

We thank members of the Ay and Ozbudak laboratories for their comments. We are grateful to Julian Lewis and François Giudicelli for providing the *Tg(hsp70l:HA-her7)* transgenic line and Spartak Kalinin for fish care. We thank Anja Hanisch, Dan Schult, Ken Belanger, Stuart Newman and Julian Lewis for critical reading of the manuscript.

Funding

This study was supported by the Colgate University NASC Division funds (A.A.) and an Alfred P. Sloan Foundation Research Fellowship (E.M.O.).

Competing interests statement

The authors declare no competing financial interests.

Author contributions

A.A. and E.M.O. designed the project and built the mathematical model. A.A., A.S. and J.H. wrote the computational code and run the simulations. S.K. and E.M.O. designed and performed the experiments. A.A., S.K., A.S., J.H. and E.M.O. wrote the manuscript.

Supplementary material

Supplementary material available online at
http://dev.biologists.org/lookup/suppl/doi:10.1242/dev.093278/-/DC1

References

Anderson, D. F. (2007). A modified next reaction method for simulating chemical systems with time dependent propensities and delays. *J. Chem. Phys.* **127**, 214107.

Buchler, N. E., Gerland, U. and Hwa, T. (2005). Nonlinear protein degradation and the function of genetic circuits. *Proc. Natl. Acad. Sci. USA* **102**, 9559-9564.

Choorapoikayil, S., Willems, B., Ströhle, P. and Gajewski, M. (2012). Analysis of her1 and her7 mutants reveals a spatio temporal separation of the somite clock module. *PLoS ONE* **7**, e39073.

Cinquin, O. (2007). Repressor dimerization in the zebrafish somitogenesis clock. *PLOS Comput. Biol.* **3**, e32.

Delaune, E. A., François, P., Shih, N. P. and Amacher, S. L. (2012). Single-cell-resolution imaging of the impact of Notch signaling and mitosis on segmentation clock dynamics. *Dev. Cell* **23**, 995-1005.

Eckalbar, W. L., Lasku, E., Infante, C. R., Elsey, R. M., Markov, G. J., Allen, A. N., Corneveaux, J. J., Losos, J. B., DeNardo, D. F., Huentelman, M. J. et al. (2012). Somitogenesis in the anole lizard and alligator reveals evolutionary convergence and divergence in the amniote segmentation clock. *Dev. Biol.* **363**, 308-319.

Gajewski, M., Sieger, D., Alt, B., Leve, C., Hans, S., Wolff, C., Rohr, K. B. and Tautz, D. (2003). Anterior and posterior waves of cyclic her1 gene expression are differentially regulated in the presomitic mesoderm of zebrafish. *Development* **130**, 4269-4278.

Giudicelli, F., Ozbudak, E. M., Wright, G. J. and Lewis, J. (2007). Setting the tempo in development: an investigation of the zebrafish somite clock mechanism. *PLoS Biol.* **5**, e150.

Goldbeter, A. and Pourquié, O. (2008). Modeling the segmentation clock as a network of coupled oscillations in the Notch, Wnt and FGF signaling pathways. *J. Theor. Biol.* **252**, 574-585.

Gomez, C., Ozbudak, E. M., Wunderlich, J., Baumann, D., Lewis, J. and Pourquié, O. (2008). Control of segment number in vertebrate embryos. *Nature* **454**, 335-339.

Hanisch, A., Holder, M. V., Choorapoikayil, S., Gajewski, M., Özbudak, E. M. and Lewis, J. (2013). The elongation rate of RNA polymerase II in zebrafish and its significance in the somite segmentation clock. *Development* **140**, 444-453.

Henry, C. A., Urban, M. K., Dill, K. K., Merlie, J. P., Page, M. F., Kimmel, C. B. and Amacher, S. L. (2002). Two linked hairy/Enhancer of split-related zebrafish genes, her1 and her7, function together to refine alternating somite boundaries. *Development* **129**, 3693-3704.

Herrgen, L., Ares, S., Morelli, L. G., Schröter, C., Jülicher, F. and Oates, A. C. (2010). Intercellular coupling regulates the period of the segmentation clock. *Curr. Biol.* **20**, 1244-1253.

Hirata, H., Bessho, Y., Kokubu, H., Masamizu, Y., Yamada, S., Lewis, J. and Kageyama, R. (2004). Instability of Hes7 protein is crucial for the somite segmentation clock. *Nat. Genet.* **36**, 750-754.

Horikawa, K., Ishimatsu, K., Yoshimoto, E., Kondo, S. and Takeda, H. (2006). Noise-resistant and synchronized oscillation of the segmentation clock. *Nature* **441**, 719-723.

Jensen, M. H., Sneppen, K. and Tiana, G. (2003). Sustained oscillations and time delays in gene expression of protein Hes1. *FEBS Lett.* **541**, 176-177.

Jiang, Y. J., Aerne, B. L., Smithers, L., Haddon, C., Ish-Horowicz, D. and Lewis, J. (2000). Notch signalling and the synchronization of the somite segmentation clock. *Nature* **408**, 475-479.

Kawamura, A., Koshida, S., Hijikata, H., Sakaguchi, T., Kondoh, H. and Takada, S. (2005). Zebrafish hairy/enhancer of split protein links FGF signaling to cyclic gene expression in the periodic segmentation of somites. *Genes Dev.* **19**, 1156-1161.

Krol, A. J., Roellig, D., Dequéant, M. L., Tassy, O., Glynn, E., Hattem, G., Mushegian, A., Oates, A. C. and Pourquié, O. (2011). Evolutionary plasticity of segmentation clock networks. *Development* **138**, 2783-2792.

Lewis, J. (2003). Autoinhibition with transcriptional delay: a simple mechanism for the zebrafish somitogenesis oscillator. *Curr. Biol.* **13**, 1398-1408.

Mara, A., Schroeder, J., Chalouni, C. and Holley, S. A. (2007). Priming, initiation and synchronization of the segmentation clock by deltaD and deltaC. *Nat. Cell Biol.* **9**, 523-530.

Momiji, H. and Monk, N. A. (2008). Dissecting the dynamics of the Hes1 genetic oscillator. *J. Theor. Biol.* **254**, 784-798.

Monk, N. A. M. (2003). Oscillatory expression of Hes1, p53, and NF-kappaB driven by transcriptional time delays. *Curr. Biol.* **13**, 1409-1413.

Oates, A. C. and Ho, R. K. (2002). Hairy/E(spl)-related (Her) genes are central components of the segmentation oscillator and display redundancy with the Delta/Notch signaling pathway in the formation of anterior segmental boundaries in the zebrafish. *Development* **129**, 2929-2946.

Ozbudak, E. M. and Lewis, J. (2008). Notch signalling synchronizes the zebrafish segmentation clock but is not needed to create somite boundaries. *PLoS Genet.* **4**, e15.

Ozbudak, E. M. and Pourquié, O. (2008). The vertebrate segmentation clock: the tip of the iceberg. *Curr. Opin. Genet. Dev.* **18**, 317-323.

Ozbudak, E. M., Thattai, M., Kurtser, I., Grossman, A. D. and van Oudenaarden, A. (2002). Regulation of noise in the expression of a single gene. *Nat. Genet.* **31**, 69-73.

Paulsson, J. (2004). Summing up the noise in gene networks. *Nature* **427**, 415-418.

Pourquié, O. (2011). Vertebrate segmentation: from cyclic gene networks to scoliosis. *Cell* **145**, 650-663.

Riedel-Kruse, I. H., Müller, C. and Oates, A. C. (2007). Synchrony dynamics during initiation, failure, and rescue of the segmentation clock. *Science* **317**, 1911-1915.

Schröter, C. and Oates, A. C. (2010). Segment number and axial identity in a segmentation clock period mutant. *Curr. Biol.* **20**, 1254-1258.

Schröter, C., Ares, S., Morelli, L. G., Isakova, A., Hens, K., Soroldoni, D., Gajewski, M., Jülicher, F., Maerkl, S. J., Deplancke, B. et al. (2012). Topology and dynamics of the zebrafish segmentation clock core circuit. *PLoS Biol.* **10**, e1001364.

Shankaran, S. S., Sieger, D., Schroter, C., Czepe, C., Pauly, M. C., Laplante, M. A., Becker, T. S., Oates, A. C. and Gajewski, M. (2007). Completing the set of h/E(spl) cyclic genes in zebrafish: her12 and her15 reveal novel modes of expression and contribute to the segmentation clock. *Dev. Biol.* **304**, 615-632.

Sieger, D., Ackermann, B., Winkler, C., Tautz, D. and Gajewski, M. (2006). her1 and her13.2 are jointly required for somitic border specification along the entire axis of the fish embryo. *Dev. Biol.* **293**, 242-251.

Trofka, A., Schwendinger-Schreck, J., Brend, T., Pontius, W., Emonet, T. and Holley, S. A. (2012). The Her7 node modulates the network topology of the zebrafish segmentation clock via sequestration of the Hes6 hub. *Development* **139**, 940-947.

Wright, G. J., Giudicelli, F., Soza-Ried, C., Hanisch, A., Ariza-McNaughton, L. and Lewis, J. (2011). DeltaC and DeltaD interact as Notch ligands in the zebrafish segmentation clock. *Development* **138**, 2947-2956.

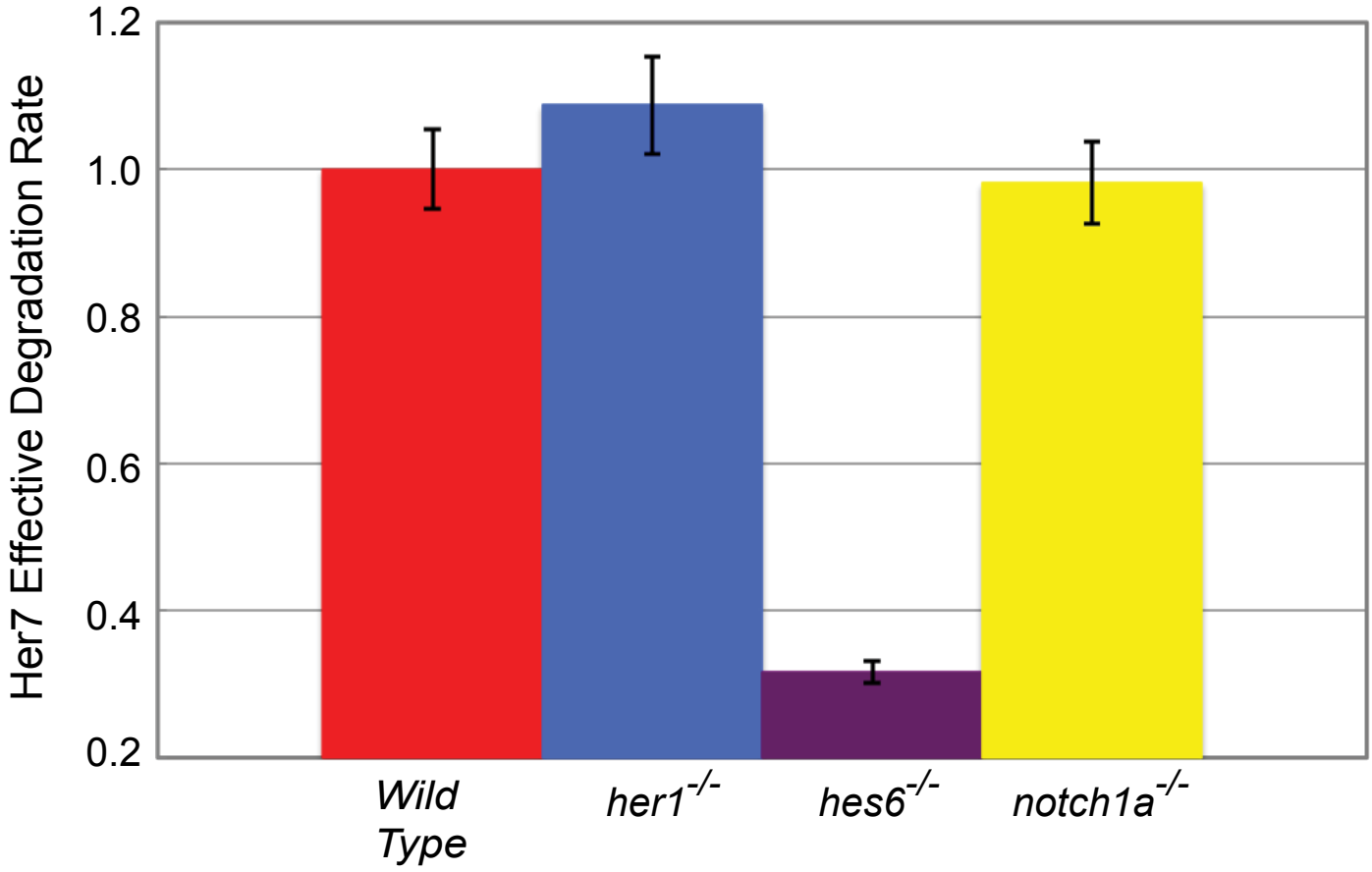

Fig. S1. Average effective degradation rate of Her7 protein in different genetic backgrounds. Error bars reprresent normalized standard errors.

Movie 1. Wild type. Simulations of *her1* mRNA levels in 4×4 cells located in the posterior PSM in wild-type embryos. Each hexagon represents a cell, with its color indicating its level of *her1* mRNA. Darker colors indicate lower levels, whereas lighter colors represent higher levels.

Movie 2. *her1*$^{-/-}$ mutant. Simulations of *her1* mRNA levels in 4×4 cells located in the posterior PSM in *her1*$^{-/-}$ mutant embryos. Each hexagon represents a cell, with its color indicating its level of *her1* mRNA. Darker colors indicate lower levels, whereas lighter colors represent higher levels.

Movie 3. *her7*$^{-/-}$ mutant. Simulations of *her1* mRNA levels in 4×4 cells located in the posterior PSM in *her7*$^{-/-}$ mutant embryos. Each hexagon represents a cell, with its color indicating its level of *her1* mRNA. Darker colors indicate lower levels, whereas lighter colors represent higher levels.

Movie 4. *hes6*$^{-/-}$ mutant. Simulations of *her1* mRNA levels in 4×4 cells located in the posterior PSM in *hes6*$^{-/-}$ mutant embryos. Each hexagon represents a cell, with its color indicating its level of *her1* mRNA. Darker colors indicate lower levels, whereas lighter colors represent higher levels.

Movie 5. *her*$^{-/-}$*;hes6*$^{-/-}$ mutant. Simulations of *her1* mRNA levels in 4×4 cells located in the posterior PSM in *her7*$^{-/-}$*;hes6*$^{-/-}$ mutant embryos. Each hexagon represents a cell, with its color indicating its level of *her1* mRNA. Darker colors indicate lower levels, whereas lighter colors represent higher levels.

Movie 6. *notch1a*$^{-/-}$ mutant. Simulations of *her1* mRNA levels in 4×4 cells located in the posteriorPSM in *notch1a*$^{-/-}$ mutant embryos. Each hexagon represents a cell, with its color indicating its level of *her1* mRNA. Darker colors indicate lower levels, whereas lighter colors represent higher levels.

Table S1. Parameter ranges and values used in the study. The initial parameter ranges (second column) were broadly selected and centered around the literature information. These ranges have been narrowed down by comparing deterministic and stochastic simulations of our model to the wild-type and mutant period, amplitude and synchronization observations (third column). One of the parameter sets that has passed these comparisons is shown in the fourth column. This parameter set has been used to create the Figs 2-4.

Parameter	Initial range	Final range	Value in Figs 2-4
psh_1	5-60	30-60	49.9139
psh_6	5-60	27-57	34.3117
psh_7	5-60	10-57	28.5626
psd	5-60	22-59	37.7828
pdh_1	0.1-0.4 1/min	0.12-0.37 1/min	0.34951
pdh_6	0.1-0.4 1/min	0.11-0.39 1/min	0.14824
pdh_7	0.1-0.4 1/min	0.11-0.4 1/min	0.249715
pdd	0.1-0.4 1/min	0.15-0.38 1/min	0.324316
msh_1	15-65	32-63	48.3084
msh_6	15-65	31-62	36.4073
msh_7	15-65	34-62	39.685
msd	15-65	31-65	60.5577
mdh_1	0.1-0.4 1/min	0.2-0.38 1/min	0.322965
mdh_6	0.1-0.4 1/min	0.13-0.39 1/min	0.146372
mdh_7	0.1-0.4 1/min	0.28-0.4 1/min	0.381738
mdd	0.1-0.4 1/min	0.12-0.39 1/min	0.352056
$pdh_{1,1}$	0.1-0.4 1/min	0.25-0.4 1/min	0.390961
$pdh_{1,6}$	0.1-0.4 1/min	0.1-0.36 1/min	0.29774
$pdh_{1,7}$	0.1-0.4 1/min	0.16-0.34 1/min	0.320157
$pdh_{6,6}$	0.1-0.4 1/min	0.11-0.34 1/min	0.268042
$pdh_{6,7}$	0.1-0.4 1/min	0.26-0.4 1/min	0.352037
$pdh_{7,7}$	0.1-0.4 1/min	0.12-0.4 1/min	0.251601
nmh_1	5-12 min	8.8-12 min	10.0213
nmh_7	5-12 min	8.6-11.6 min	10.4515
nmd	5-12 min	6.1-12 min	7.74472
nph_1	0.3-2 min	0.8-2 min	1.5398
nph_6	0.3-2 min	0.6-1.8 min	0.886233
nph_7	0.3-2 min	0.4-1.8 min	0.539972
npd	9-27 min	10-18 min	13.2661
$dah_{1,1}$	0.0003-0.03	0.005-0.03	0.0179429
$ddh_{1,1}$	0.003-0.3	0.06-0.3	0.220856
$dah_{1,6}$	0.0003-0.03	0.006-0.029	0.0270209
$ddh_{1,6}$	0.003-0.3	0.004-0.18	0.0917567
$dah_{1,7}$	0.0003-0.03	0.0006-0.009	0.00120525
$ddh_{1,7}$	0.003-0.3	0.03-0.28	0.258167
$dah_{6,6}$	0.0003-0.03	0.001-0.016	0.0148271
$ddh_{6,6}$	0.003-0.3	0.05-0.29	0.251173
$dah_{6,7}$	0.0003-0.03	0.007-0.03	0.0216093
$ddh_{6,7}$	0.003-0.3	0.03-0.3	0.188923
$dah_{7,7}$	0.0003-0.03	0.002-0.024	0.0202756
$ddh_{7,7}$	0.003-0.3	0.07-0.3	0.161018
$critph_{1,1}$	30-1500	160-720	587.298
$critph_{6,7}$	30-1500	200-920	769.628
critpd	30-1500	240-720	490.254

APPENDIX S1

DELAY DIFFERENTIAL EQUATION (DDE) MODEL

A. INTRODUCTION

A.1. Mass Action Kinetics

Mass action kinetics describe the behavior of reactants and products in chemical reactions. The behavior is described as an equation where the rate of the reaction is directly proportional to the concentration of reactants. We have used mass action kinetics to create our delay differential equation model.

Chemical reactions can be classified according to the dependency of the reaction rate on the number of reactants, which is called the order of a reaction. In a zero order reaction, the reaction rate does not depend on the concentration of reactants. In first and second order reactions, the reaction rates depend on the concentrations of one reactant or two reactants, respectively. The reaction rates for zero, first and second order reactions can be written as described in the table below. Here, r represents the unit rate for each reaction.

Zero Order Reaction	$\varnothing \xrightarrow{r} P$	Reaction Rate = r
First Order Reaction	$R_1 \xrightarrow{r} P$	Reaction Rate = $r \cdot R_1$
Second Order Reaction	$R_1 + R_2 \xrightarrow{r} P$	Reaction Rate = $r \cdot R_1 \cdot R_2$

In our model *hes6* mRNA synthesis is a zero order reaction. Translation of mRNA to protein, degradation of mRNA and protein, and dimer dissociation reactions are first order reactions. Dimer association reactions are second order reactions.

A.2. Model Variables

In the delay differential equation model, mh_i where $i \in \{1, 7, 6\}$ and md represent the number of mRNA molecules of *her1*, *her7*, *hes6* and *deltaC*, respectively. ph_i where $i \in \{1, 7, 6\}$ and pd represent the number of protein monomers of Her1, Her7, Hes6 and DeltaC, respectively. $ph_{i,j}$ where $i \leq j$ and $i,j \in \{1, 7, 6\}$ represent the number of molecules of Her1-Her1, Her1-Her7, Her1-Hes6, Her7-Her7, Her7-Hes6 and Hes6-Hes6 dimers. In the model equations, we represent the k^{th} cell as c_k and time as t.

B. MONOMER PROTEIN LEVELS

B.1. Her1 Monomer Protein Levels

[Rate of Change in Her1 Monomer Protein Levels] = [Her1 Protein Synthesis] – [Her1 Protein Degradation] + [Her1-Her1 Dimer Dissociation] + [Her1-Her7 Dimer Dissociation] + [Her1-Hes6 Dimer Dissociation] – [Her1-Her1 Dimer Association] – [Her1-Her7 Dimer Association] – [Her1-Hes6 Dimer Association]

(i) Rate of Change in Her1 Monomer Protein Levels = $\frac{\partial ph_1(c_k,t)}{\partial t}$.

(ii) Her1 Protein Synthesis ($mh_1 \rightarrow ph_1$): $psh_1 \cdot mh_1(c_k,t\text{-}nph_1)$ where psh_1 represents the Her1 protein synthesis rate and nph_1 represents the Her1 translation time delay.

(iii) Her1 Protein Degradation ($ph_1 \rightarrow \varnothing$): $pdh_1 \cdot ph_1(c_k,t)$ where pdh_1 represents the Her1 protein degradation rate.

(iv) Her1-Her1 Dimer Dissociation ($ph_{1,1} \rightarrow ph_1 + ph_1$): $2 \cdot ddh_{1,1} \cdot ph_{1,1}(c_k,t)$ where $ddh_{1,1}$ represents the Her1-Her1 dimer dissociation rate. We use 2 in the equation since a Her1-Her1 dimer is formed by two Her1 monomers.

(v) Her1-Her7 Dimer Dissociation ($ph_{1,7} \rightarrow ph_1 + ph_7$): $ddh_{1,7} \cdot ph_{1,7}(c_k,t)$ where $ddh_{1,7}$ represents the Her1-Her7 dimer dissociation rate.

(vi) Her1-Hes6 Dimer Dissociation ($ph_{1,6} \rightarrow ph_1 + ph_6$): $ddh_{1,6} \cdot ph_{1,6}(c_k,t)$ where $ddh_{1,6}$ represents the Her1-Hes6 dimer dissociation rate.

(vii) Her1-Her1 Dimer Association ($ph_1 + ph_1 \rightarrow ph_{1,1}$): $2 \cdot dah_{1,1} \cdot ph_1(c_k,t) \cdot ph_1(c_k,t)$ where $dah_{1,1}$ represents the Her1-Her1 dimer association rate. We use 2 in the equation since a Her1-Her1 dimer is formed by two Her1 monomers.

(viii) Her1-Her7 Dimer Association ($ph_1 + ph_7 \rightarrow ph_{1,7}$): $dah_{1,7} \cdot ph_1(c_k,t) \cdot ph_7(c_k,t)$ where $dah_{1,7}$ represents the Her1-Her7 dimer association rate.

(ix) Her1-Hes6 Dimer Association ($ph_1 + ph_6 \rightarrow ph_{1,6}$): $dah_{1,6} \cdot ph_1(c_k,t) \cdot ph_6(c_k,t)$ where $dah_{1,6}$ represents the Her1-Hes6 dimer association rate.

Combining (i)-(ix) we obtain the equation for the rate of change of Her1 monomer protein levels.

$$\frac{\partial ph_1(c_k,t)}{\partial t} = psh_1 \cdot mh_1(c_k,t\text{-}nph_1) - pdh_1 \cdot ph_1(c_k,t) + 2 \cdot ddh_{1,1} \cdot ph_{1,1}(c_k,t) + ddh_{1,7} \cdot ph_{1,7}(c_k,t)$$
$$+ ddh_{1,6} \cdot ph_{1,6}(c_k,t) - 2 \cdot dah_{1,1} \cdot ph_1(c_k,t) \cdot ph_1(c_k,t) - dah_{1,7} \cdot ph_1(c_k,t) \cdot ph_7(c_k,t) - dah_{1,6} \cdot ph_1(c_k,t) \cdot ph_6(c_k,t)$$

If we use the summation symbol ($\sum$) and define $C_{1,1} = 2$, $C_{1,7} = 1$ and $C_{1,6} = 1$ we can rewrite this equation as

$$\frac{\partial ph_1(c_k,t)}{\partial t} = psh_1 \cdot mh_1(c_k,t\text{-}nph_1) - pdh_1 \cdot ph_1(c_k,t) + \sum_{j\in\{1,7,6\}} C_{1,j} \cdot [ddh_{1,j} \cdot ph_{1,j}(c_k,t) - dah_{1,j} \cdot ph_1(c_k,t) \cdot ph_j(c_k,t)]$$

B.2. Her/Hes Monomer Protein Levels (General Formula)

Similar steps to the Her1 derivation can be used to derive the equations for Her7 and Hes6 monomer protein levels. We can combine the equations for Her1, Her7 and Hes6 monomer levels in one equation.

$$\frac{\partial ph_i(c_k,t)}{\partial t} = psh_i \cdot mh_i(c_k,t\text{-}nph_i) - pdh_i \cdot ph_i(c_k,t) + \sum_{\substack{i\le j \text{ and} \\ i,j\in\{1,7,6\}}} C_{i,j} \cdot [ddh_{i,j} \cdot ph_{i,j}(c_k,t) - dah_{i,j} \cdot ph_i(c_k,t) \cdot ph_j(c_k,t)]$$

where $C_{i,j} = 2$, if $i=j$ and $C_{i,j} = 1$, if $i \neq j$

In this equation psh_i and pdh_i where $i \in \{1, 7, 6\}$ represent the Her1, Her7 and Hes6 protein synthesis and degradation rates, respectively. $dah_{i,j}$ and $ddh_{i,j}$ where $i \le j$ and $i,j \in \{1, 7, 6\}$ represent the Her1-Her1, Her1-Her7, Her1-Hes6, Her7-Her7, Her7-Hes6 and Hes6-Hes6 dimer association and dissociation rates, respectively.

B.3. DeltaC Protein Levels

[Rate of Change in DeltaC Protein Levels] = [DeltaC Protein Synthesis] – [DeltaC Protein Degradation]

(i) Rate of Change in DeltaC Protein Levels = $\frac{\partial pd(c_k,t)}{\partial t}$.

(ii) DeltaC Protein Synthesis ($md \rightarrow pd$) : $psd \cdot md(c_k,t\text{-}npd)$ where psd represents the DeltaC protein synthesis rate and npd represents the DeltaC translation time delay.

(iii) DeltaC Protein Degradation ($pd \rightarrow \varnothing$) : $pdd \cdot pd(c_k,t)$ where pdd represents the DeltaC protein degradation rate.

Combining (i)-(iii) we obtain the equation for the rate of change of DeltaC protein levels.

$$\frac{\partial pd(c_k,t)}{\partial t} = psd \cdot md(c_k,t\text{-}npd) - pdd \cdot pd(c_k,t)$$

C. DIMER PROTEIN LEVELS

C.1. Her1-Her1 Dimer Levels

[Rate of Change in Her1-Her1 Dimer Levels] = [Her1-Her1 Dimer Association] – [Her1-Her1 Dimer Dissociation] – [Her1-Her1 Dimer Degradation]

(i) Rate of Change in Her1 Dimer Protein Levels = $\frac{\partial ph_{1,1}(c_k,t)}{\partial t}$.

(ii) Her1-Her1 Dimer Association ($ph_1 + ph_1 \rightarrow ph_{1,1}$) : $dah_{1,1} \cdot ph_1(c_k,t) \cdot ph_1(c_k,t)$ where $dah_{1,1}$ represents the Her1-Her1 dimer association rate.

(iii) Her1-Her1 Dimer Dissociation ($ph_{1,1} \rightarrow ph_1 + ph_1$) : $ddh_{1,1} \cdot ph_{1,1}(c_k,t)$ where $ddh_{1,1}$ represents the Her1-Her1 dimer dissociation rate.

(iv) Her1-Her1 Dimer Degradation ($ph_{1,1} \rightarrow \varnothing$) : $pdh_{1,1} \cdot ph_{1,1}(c_k,t)$ where $pdh_{1,1}$ represents the Her1-Her1 dimer degradation rate.

Combining (i)-(iv) we obtain the equation for the rate of change of Her1-Her1 dimer levels.

$$\frac{\partial ph_{1,1}(c_k,t)}{\partial t} = dah_{1,1} \cdot ph_1(c_k,t) \cdot ph_1(c_k,t) - ddh_{1,1} \cdot ph_{1,1}(c_k,t) - pdh_{1,1} \cdot ph_{1,1}(c_k,t)$$

C.2. Her/Hes Dimer Levels

Similar steps to the above derivation can be used to derive the equations for Her1-Her7, Her1-Hes6, Her7-Her7, Her7-Hes6 and Hes6-Hes6 dimer levels. We can combine the equations for Her1-Her1, Her1-Her7, Her1-Hes6, Her7-Her7, Her7-Hes6 and Hes6-Hes6 dimer levels in one equation.

$$\frac{\partial ph_{i,j}(c_k,t)}{\partial t} = dah_{i,j} \cdot ph_i(c_k,t) \cdot ph_j(c_k,t) - ddh_{i,j} \cdot ph_{i,j}(c_k,t) - pdh_{i,j} \cdot ph_{i,j}(c_k,t)$$

$$\text{where } i \leq j \text{ and } i, j \in \{1, 7, 6\}$$

In this equation $dah_{i,j}$, $ddh_{i,j}$ and $pdh_{i,j}$ where $i \leq j$ and $i,j \in \{1, 7, 6\}$ represent the Her1-Her1, Her1-Her7, Her1-Hes6, Her7-Her7, Her7-Hes6 and Hes6-Hes6 dimer association, dissociation and degradation rates, respectively.

D. mRNA LEVELS

D.1. *hes6* mRNA Levels

[Rate of Change in *hes6* mRNA Levels] = [*hes6* mRNA Synthesis] – [*hes6* mRNA Degradation]

(i) Rate of Change in *hes6* mRNA Levels = $\frac{\partial mh_6(c_k,t)}{\partial t}$.

(ii) *hes6* mRNA Synthesis ($\varnothing \rightarrow mh_6$) : msh_6 where msh_6 represents the maximum *hes6* mRNA synthesis rate. Since transcription of *hes6* is not regulated by Notch signaling and Her/Hes transcription factors in the posterior presomitic mesoderm, transcription rate is assumed to be constant (msh_6) in our model.

(iii) *hes6* mRNA Degradation ($mh_6 \rightarrow \varnothing$) : $mdh_6 \cdot mh_6(c_k,t)$ where mdh_6 represents the *hes6* mRNA degradation rate.

Combining (i)-(iii) we obtain the equation for the rate of change of *hes6* mRNA levels.

$$\frac{\partial mh_6(c_k,t)}{\partial t} = msh_6 - mdh_6 \cdot mh_6(c_k,t)$$

D.2. *her1* mRNA Levels

[Rate of Change in *her1* mRNA Levels] = [*her1* mRNA Synthesis] – [*her1* mRNA Degradation]

(i) Rate of Change in *her1* mRNA Levels = $\frac{\partial mh_1(c_k,t)}{\partial t}$.

(ii) *her1* mRNA Synthesis ($\varnothing \rightarrow mh_1$) :

$$msh_1 \frac{1+[\frac{1}{6}\sum_{c_n \in N} \frac{pd(c_n,t-nmh_1)}{critpd}]}{1+[\frac{1}{6}\sum_{c_n \in N} \frac{pd(c_n,t-nmh_1)}{critpd}]+[\frac{ph_{1,1}(c_k,t-nmh_1)}{critph_{1,1}}]^2+[\frac{ph_{6,7}(c_k,t-nmh_1)}{critph_{6,7}}]^2}$$ where msh_1 represents the maximum *her1* mRNA synthesis rate, $critph_{1,1}$, $critph_{6,7}$ and $critpd$ are DNA-binding dissociation constants for Her1-Her1, Her7-Hes6 and NICD, respectively. Also N represents all the neighbors of the k^{th} cell and nmh_1 represents *her1* mRNA transcription time delay.

Form of Transcription Term:

Transcriptions of *her1* and *her7* are repressed by Her-Her1 and Her7-Hes6 dimer proteins but activated by Notch signaling. The activity of Notch signaling is proportional to the levels of DeltaC protein.

In our model, we assume that transcription rate of *her1* is proportional to the ratio:

$$\frac{\text{"DNA states free of repressors"}}{\text{"Total DNA state"}}$$

"DNA states free of repressor" = "Vacant DNA" + "Activator (NICD)-bound DNA"

"Total DNA states" = "Vacant DNA" + "NICD-bound DNA" + "Her1-Her1 homodimer bound DNA" + "Her7-Hes6 heterodimer bound DNA"

Please note that in our model it is assumed that two Her1-Her1, Her7-Hes6 dimers bind to DNA as a tetramer and NICD, which is activated by DeltaC protein from six neighboring cells, bind as a monomer. Because of that, we square the terms for Her1-Her1 and Her7-Hes6 dimers but not DeltaC term.

(iii) *her1* mRNA Degradation ($mh_1 \rightarrow \varnothing$) : $mdh_1 \cdot mh_1(c_k,t)$ where mdh_1 represents the *her1* mRNA degradation rate.

Combining (i)-(iii) we obtain the equation for the rate of change of *her1* mRNA levels.

$$\frac{\partial mh_1(c_k,t)}{\partial t} = msh_1 \frac{1+[\frac{1}{6}\sum_{c_n \in N} \frac{pd(c_n,t\text{-}nmh_1)}{critpd}]}{1+[\frac{1}{6}\sum_{c_n \in N} \frac{pd(c_n,t\text{-}nmh_1)}{critpd}]+[\frac{ph_{1,1}(c_k,t\text{-}nmh_1)}{critph_{1,1}}]^2+[\frac{ph_{6,7}(c_k,t\text{-}nmh_1)}{critph_{6,7}}]^2} - mdh_1 \cdot mh_1(c_k,t)$$

D.3. *her1* and *her7* mRNA Levels

Similar steps to the *her1* derivation can be used to derive the equations for *her7* mRNA levels. We can combine the equations for *her1* and *her7* mRNA levels in one equation.

$$\frac{\partial mh_i(c_k,t)}{\partial t} = msh_i \frac{1+[\frac{1}{6}\sum_{c_n \in N} \frac{pd(c_n,t\text{-}nmh_i)}{critpd}]}{1+[\frac{1}{6}\sum_{c_n \in N} \frac{pd(c_n,t\text{-}nmh_i)}{critpd}]+[\frac{ph_{1,1}(c_k,t\text{-}nmh_i)}{critph_{1,1}}]^2+[\frac{ph_{6,7}(c_k,t\text{-}nmh_i)}{critph_{6,7}}]^2} - mdh_i \cdot mh_i(c_k,t)$$

where $i \in \{1, 7\}$

In this equation msh_i and mdh_i where $i \in \{1, 7\}$ represent the *her1* and *her7* mRNA max synthesis rate and degradation rate, respectively. $critph_{1,1}$, $critph_{6,7}$ and critpd are DNA-binding dissociation constants for Her1-Her1, Her7-Hes6 and NICD, respectively. N represents

all the neighbors of the k^{th} cell and nmh_i where $i \in \{1, 7\}$ represents *her1* and *her7* mRNA transcription time delay.

D.4. *deltaC* mRNA Levels

[Rate of Change in *deltaC* mRNA Levels] = [*deltaC* mRNA Synthesis] – [*deltaC* mRNA Degradation]

(i) Rate of Change in *deltaC* mRNA Levels = $\frac{\partial md(c_k,t)}{\partial t}$.

(ii) *deltaC* mRNA Synthesis ($\varnothing \rightarrow md$) : $msd\frac{1}{1+[\frac{ph_{1,1}(c_k,t\text{-}nmd)}{critph_{1,1}}]^2+[\frac{ph_{6,7}(c_k,t\text{-}nmd)}{critph_{6,7}}]^2}$ where

msd represents the maximum *deltaC* mRNA synthesis rate. $critph_{1,1}$ and $critph_{6,7}$ are DNA-binding dissociation constants for Her1-Her1 and Her7-Hes6. nmd represents *deltaC* mRNA transcription time delay.

Form of Transcription Term:

Transcription of *deltaC* is repressed by Her-Her1 and Her7-Hes6 dimer proteins. In our model, we assume that transcription rate of *deltaC* is proportional to the ratio:

$$\frac{\text{"DNA states free of repressors"}}{\text{"Total DNA state"}}$$

"DNA states free of repressor" = "Vacant DNA"

"Total DNA states" = "Vacant DNA" + "Her1-Her1 homodimer bound DNA" + "Her7-Hes6 heterodimer bound DNA"

Please note that in our model it is assumed that two Her1-Her1 and Her7-Hes6 dimers bind to DNA as a tetramer. Because of that we square the terms for Her1-Her1 and Her7-Hes6 dimers.

(iii) *deltaC* mRNA Degradation ($md \rightarrow \varnothing$) : $mdd \cdot md(c_k,t)$ where mdd represents the *deltaC* mRNA degradation rate.

Combining (i)-(iii) we obtain the equation for the rate of change of *hes6* mRNA levels.

$$\frac{\partial md(c_k,t)}{\partial t}=msd\frac{1}{1+[\frac{ph_{1,1}(c_k,t\text{-}nmd)}{critph_{1,1}}]^2+[\frac{ph_{6,7}(c_k,t\text{-}nmd)}{critph_{6,7}}]^2} - mdd \cdot md(c_k,t)$$

STOCHASTIC SIMULATIONS

Reactions and propensities used in stochastic simulations.

Reaction (for each cell)	Propensity (for each cell c_k)
Reaction 1: $mh_1 \rightarrow ph_1$ (Her1 protein synthesis)	$a_1(c_k) = psh_1 \cdot mh_1(c_k)$
Reaction 2: $ph_1 \rightarrow \varnothing$ (Her1 protein degradation)	$a_2(c_k) = pdh_1 \cdot ph_1(c_k)$
Reaction 3: $ph_1 + ph_1 \rightarrow ph_{1,1}$ (Her1-Her1 dimer association)	$a_3(c_k) = dah_{1,1} \cdot ph_1(c_k) \cdot (ph_1(c_k)-1)/2$
Reaction 4: $ph_{1,1} \rightarrow ph_1 + ph_1$ (Her1-Her1 dimer dissociation)	$a_4(c_k) = ddh_{1,1} \cdot ph_{1,1}(c_k)$
Reaction 5: $ph_1 + ph_7 \rightarrow ph_{1,7}$ (Her1-Her7 dimer association)	$a_5(c_k) = dah_{1,7} \cdot ph_1(c_k) \cdot ph_7(c_k)$
Reaction 6: $ph_{1,7} \rightarrow ph_1 + ph_7$ (Her1-Her7 dimer dissociation)	$a_6(c_k) = ddh_{1,7} \cdot ph_{1,7}(c_k)$
Reaction 7: $ph_1 + ph_6 \rightarrow ph_{1,6}$ (Her1-Hes6 dimer association)	$a_7(c_k) = dah_{1,6} \cdot ph_1(c_k) \cdot ph_6(c_k)$
Reaction 8: $ph_{1,6} \rightarrow ph_1 + ph_6$ (Her1-Hes6 dimer dissociation)	$a_8(c_k) = ddh_{1,6} \cdot ph_{1,6}(c_k)$
Reaction 9: $mh_7 \rightarrow ph_7$ (Her7 protein synthesis)	$a_9(c_k) = psh_7 \cdot mh_7(c_k)$
Reaction 10: $ph_7 \rightarrow \varnothing$ (Her7 protein degradation)	$a_{10}(c_k) = pdh_7 \cdot ph_7(c_k)$
Reaction 11: $ph_7 + ph_7 \rightarrow ph_{7,7}$ (Her7-Her7 dimer association)	$a_{11}(c_k) = dah_{7,7} \cdot ph_7(c_k) \cdot (ph_7(c_k)-1)/2$
Reaction 12: $ph_{7,7} \rightarrow ph_7 + ph_7$ (Her7-Her7 dimer dissociation)	$a_{12}(c_k) = ddh_{7,7} \cdot ph_{7,7}(c_k)$
Reaction 13: $ph_7 + ph_6 \rightarrow ph_{6,7}$ (Her7-Hes6 dimer association)	$a_{13}(c_k) = dah_{6,7} \cdot ph_7(c_k) \cdot ph_6(c_k)$
Reaction 14: $ph_{6,7} \rightarrow ph_7 + ph_6$ (Her7-Hes6 dimer dissociation)	$a_{14}(c_k) = ddh_{6,7} \cdot ph_{6,7}(c_k)$
Reaction 15: $mh_6 \rightarrow ph_6$ (Hes6 protein synthesis)	$a_{15}(c_k) = psh_6 \cdot mh_6(c_k)$
Reaction 16: $ph_6 \rightarrow \varnothing$ (Hes6 protein degradation)	$a_{16}(c_k) = pdh_6 \cdot ph_6(c_k)$
Reaction 17: $ph_6 + ph_6 \rightarrow ph_{6,6}$ (Hes6-Hes6 dimer association)	$a_{17}(c_k) = dah_{6,6} \cdot ph_6(c_k) \cdot (ph_6(c_k)-1)/2$
Reaction 18: $ph_{6,6} \rightarrow ph_6 + ph_6$ (Hes6-Hes6 dimer dissociation)	$a_{18}(c_k) = ddh_{6,6} \cdot ph_{6,6}(c_k)$
Reaction 19: $ph_{1,1} \rightarrow \varnothing$ (Her1-Her1 dimer degradation)	$a_{19}(c_k) = pdh_{1,1} \cdot ph_{1,1}(c_k)$
Reaction 20: $ph_{1,7} \rightarrow \varnothing$ (Her1-Her7 dimer degradation)	$a_{20}(c_k) = pdh_{1,7} \cdot ph_{1,7}(c_k)$
Reaction 21: $ph_{1,6} \rightarrow \varnothing$ (Her1-Hes6 dimer degradation)	$a_{21}(c_k) = pdh_{1,6} \cdot ph_{1,6}(c_k)$
Reaction 22: $ph_{7,7} \rightarrow \varnothing$ (Her7-Her7 dimer degradation)	$a_{22}(c_k) = pdh_{7,7} \cdot ph_{7,7}(c_k)$
Reaction 23: $ph_{6,7} \rightarrow \varnothing$ (Her7-Hes6 dimer degradation)	$a_{23}(c_k) = pdh_{6,7} \cdot ph_{6,7}(c_k)$
Reaction 24: $ph_{6,6} \rightarrow \varnothing$ (Hes6-Hes6 dimer degradation)	$a_{24}(c_k) = pdh_{6,6} \cdot ph_{6,6}(c_k)$
Reaction 25: md $\rightarrow$ pd (Delta protein synthesis)	$a_{25}(c_k) = psd \cdot md(c_k)$
Reaction 26: pd $\rightarrow \varnothing$ (Delta protein degradation)	$a_{26}(c_k) = pdd \cdot pd(c_k)$
Reaction 27: $\varnothing \rightarrow mh_1$ (*her*1 mRNA synthesis)	$a_{27}(c_k) = fh_1$
Reaction 28: $mh_1 \rightarrow \varnothing$ (*her*1 mRNA degradation)	$a_{28}(c_k) = mdh_1 \cdot mh_1(c_k)$
Reaction 29: $\varnothing \rightarrow mh_7$ (*her*7 mRNA synthesis)	$a_{29}(c_k) = fh_7$
Reaction 30: $mh_7 \rightarrow \varnothing$ (*her*7 mRNA degradation)	$a_{30}(c_k) = mdh_7 \cdot mh_7(c_k)$
Reaction 31: $\varnothing \rightarrow mh_6$ (*hes*6 mRNA synthesis)	$a_{31}(c_k) = psh_6$
Reaction 32: $mh_6 \rightarrow \varnothing$ (*hes*6 mRNA degradation)	$a_{32}(c_k) = mdh_6 \cdot mh_6(c_k)$
Reaction 33: $\varnothing \rightarrow$ md (*deltaC* mRNA synthesis)	$a_{33}(c_k) = fd$
Reaction 34: md $\rightarrow \varnothing$ (*deltaC* mRNA degradation)	$a_{34}(c_k) = mdd \cdot md(c_k)$

Transcription of *her1*, *her7* and *deltaC* mRNAs have been approximated by the following functions in stochastic simulations.

Genes	Transcription Term
her1	$fh_1 = msh_1 \dfrac{1+[\frac{1}{6}\sum_{c_n \in N} \frac{pd(c_n)}{critpd}]}{1+[\frac{1}{6}\sum_{c_n \in N} \frac{pd(c_n)}{critpd}]+[\frac{ph_{1,1}(c_k)}{critph_{1,1}}]^2+[\frac{ph_{6,7}(c_k)}{critph_{6,7}}]^2}$
her7	$fh_7 = msh_7 \dfrac{1+[\frac{1}{6}\sum_{c_n \in N} \frac{pd(c_n)}{critpd}]}{1+[\frac{1}{6}\sum_{c_n \in N} \frac{pd(c_n)}{critpd}]+[\frac{ph_{1,1}(c_k)}{critph_{1,1}}]^2+[\frac{ph_{6,7}(c_k)}{critph_{6,7}}]^2}$
deltaC	$fd = msd \cdot \dfrac{1}{1+[\frac{ph_{1,1}(c_k)}{critph_{1,1}}]^2+[\frac{ph_{6,7}(c_k)}{critph_{6,7}}]^2}$
where N represents all the neighbors of the k^{th} cell (c_k).	